JÖNKÖPING UNIVERSITY
School of Engineering

Licentiate Thesis

Al-7Si-Mg Semi-Solid Castings – Microstructure and Mechanical Properties

Jorge Santos

ABSTRACT

The vehicles industry is facing increasing demands for fuel efficiency and cost reduction due to environmental legislation, sustainability and customer demands. Therefore, there is a great need to develop and produce lightweight components by using materials and processes that offer higher specific strength and/or design optimization. Semi-solid aluminium casting offers design freedom and castings with lower shrinkage and gas entrapment defects compared to high pressure die castings. The lack of understanding of microstructure and defect formation, and design data, for semi-solid castings is a barrier for foundries and designers in the vehicles industry to use semi-solid castings.

In this study, the effect of two grain refiners on slurry formation and surface segregation of semi-solid Al-7Si-0.3Mg castings produced by the Rheometal™ process was evaluated. The influence of grain refinement on primary α-Al grain size, shape factor and solid fraction was analysed in addition to the solute content of the surface segregation layer.

The influence of magnesium on the formation of intermetallic phases during solidification and the heat treatment response of Al-7Si-Mg semi-solid castings was investigated. The magnesium content was varied from 0.3 to 0.6wt.% and the semi-solid castings were analysed in the T5 and T6 conditions. Energy dispersive spectroscopy was used to identify the intermetallic phases formed during solidification. Tensile testing was performed and the results were correlated to the magnesium and silicon concentration measured in the interior of the α-Al globules formed during slurry preparation.

The results suggest that the addition of grain refiner decreases the solid fraction obtained in the Rheometal™ process. However, no significant effect was observed on the α-Al grain size and shape factor.

A good correlation was obtained between the magnesium concentration in the interior of the α-Al globules formed during slurry preparation and the offset yield strength for all alloys. The low magnesium solubility in α-Al at temperatures in the solidification range of the Al-7Si-Mg alloys is suggested to be the reason for the low hardening response for the T5 heat treatment compared to the T6 condition.

Keywords: Rheometal™ process; semi-solid casting; aluminium alloys; grain refinement; segregation; intermetallic phases; heat treatment; mechanical properties.

ACKNOWLEDGEMENTS

Jorge Santos

Jönköping 2018

iv

SUPPLEMENTS

The following supplements constitute the basis of this thesis:

Supplement I Jorge Santos, Lothar H. Kallien, Anders E. W. Jarfors, Arne K. Dahle; Influence of grain refinement on slurry formation and surface segregation in Al-7Si-0.3Mg semi-solid castings.

Manuscript. Submitted for journal publication.

Jorge Santos was the main author and performed the experimental work. Lothar H. Kallien designed and assisted during experimental work and advice regarding the work. Anders E. W. Jarfors and Arne K. Dahle contributed with analysis of the results and advice regarding the work.

Supplement II Jorge Santos, Anders E. W. Jarfors, Arne K. Dahle; The effect of magnesium on the intermetallic phases and heat treatment response of cast Al-7Si-Mg.

Manuscript.

Jorge Santos was the main author and performed the experimental work. Anders E. W. Jarfors and Arne K. Dahle contributed with advice regarding the work.

Supplement III Jorge Santos, Anders E. W. Jarfors, Arne K. Dahle; Filling, feeding and defect formation of thick-walled AlSi7Mg0.3 semi-solid castings.

Presented in the 14th International Conference on Semi Solid Processing of Alloys and Composites, October 23rd-27th, Salt Lake City, Utah, USA. Published in Solid State Phenomena, Trans Tech Publications, 2016. Vol. 256, pp. 222-227.

Jorge Santos was the main author and performed the experimental work. Anders E. W. Jarfors and Arne K. Dahle contributed with advice regarding the work.

TABLE OF CONTENTS

CHAPTER I

INTRODUCTION

CHAPTER INTRODUCTION

In this chapter the subject area is introduced and its relation its relation to increased requirements of sustainable solutions in transport.

1.1 BACKGROUND

The viscosity of a metal in the semi-solid range is shear rate and time dependent [1–3]. When a partially solidified metal with non-dendritic crystals is sheared after being stand for a while, the viscosity decreases with time until reach the new steady-state point. However, if it is allowed to stand after being sheared, the viscosity increases [4]. The discovered of the thixotropic behaviour of semi-solid metal alloys started the development of Semi-Solid Metal (SSM) casting [1]. In the SSM casting, a so-called slurry, globular crystals dispersed in the liquid, is injected into a die-cavity to produce castings. This process has advantages in comparison to High Pressure Die Casting (HPDC) such as less gas entrapment and shrinkage porosity related defects [4]. Therefore, the occurrence of blistering during T6 heat treatment or welding is reduced for SSM castings in comparison to HPDC [5].

The reduction of vehicle emissions has received increased attraction for the improvement of the Earth sustainability. European Union legislation has already targeted the emissions of vehicles for 2020 [6]. Therefore, the reduction of vehicles weight with the introduction of lightweight components is one possible solution. In a life cycle assessment perspective, there is environmental benefits of using lightweight aluminium castings in commercial vehicles [6].

Al-7Si-0.3Mg SSM castings are used for heavy-duty truck structural applications with cost savings compared to gravity and low pressure die casting processes [7]. Additionally, aluminium SSM castings replace spheroidal cast iron with weight reduction [7]. The ability to produce reliable thick-wall castings that can undergo T5 or T6 heat treatments may be required for structural applications. Additionally, such applications experience fatigue in service and the control of microstructure (grain size, intermetallic phases, eutectic silicon), and defect formation, becomes critical. Therefore, the understanding of the microstructure, defect formation and the response of SSM castings to heat treatment is essential to design SSM castings for high demanding structural applications.

1.2 ALUMINIUM ALLOYS
1.2.1 Al-7Si-Mg cast alloys

Al-7Si-Mg cast alloys have good castability, corrosion resistance and high specific strength [8–11]. Magnesium is added to increase the hardening response during artificial aging [12–14]. These alloys generally contain iron as impurity that during solidification can form together with other chemical elements intermetallic phases that can be detrimental to the mechanical properties [15]. The most common iron-rich intermetallic phases formed during solidification of Al-7Si-Mg alloys are β-Al_5FeSi and π–$Al_8FeMg_3Si_6$ [14,16]. The analysis of the phases formed during solidification of these alloys generally requires the usage of the quaternary Al-Fe-Mg-Si phase diagram [17].

Figure 1 shows the polythermal vertical section of the Al-Fe-Mg-Si phase diagram calculated using ThermoCalc™. Within the composition range of the most common alloys, A356 and A357, the variation of silicon content does not change the phases formed during solidification [17]. Thereby, a constant silicon concentration, as shown in Figure 1, can be used to analyse the phases formed during solidification in these alloys [17].
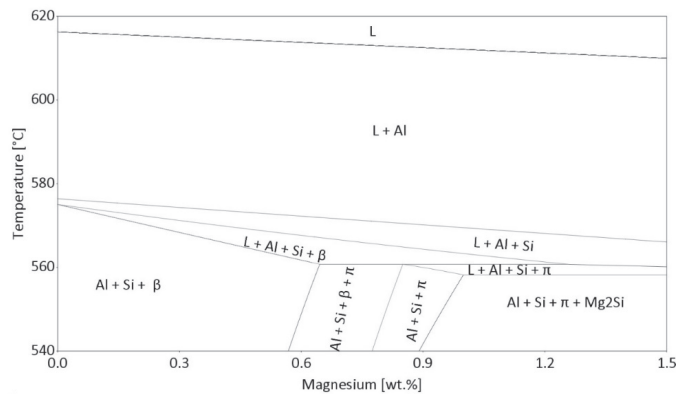
Figure 1: Polythermal vertical section of the Al-7Si-Mg-0.14Fe phase diagram. β – Al_5FeSi and π – $Al_8FeMg_3Si_6$ [18].

Typically, π-$Al_8FeMg_3Si_6$ and Mg_2Si Chinese script phases are both obtained in addition to the β- Al_5FeSi platelets in Al-7Si-Mg cast alloys [8,19,20]. The peritectic reaction that results in the formation of the π-$Al_8FeMg_3Si_6$ phase occurs due to non-equilibrium solidification in Al-7Si-Mg alloys up to 0.6wt.% magnesium [17].

The typical solidification sequence of Al-7Si-Mg cast alloys is described by Wang and Davidson [8] and Bäckerud et al. [21] as follows; the solidification starts with the primary α-Al formation followed by the binary α-Al + Si and ternary Al + Si + β eutectics; subsequently, the peritectic reaction L + β ⇔ Al + Si + π occurs and the solidification ends with the ternary Al + Si + Mg_2Si followed by the quaternary Al + Si + Mg_2Si + π eutectic formations. The increase of both iron and magnesium contents

in the Al-7Si-Mg alloys increase the amount of π-$Al_8FeMg_3Si_6$ phase formed during solidification [16].

Samuel et al. [22] reported that the strontium addition can result in a significant reduction of the β-Al_5FeSi phase fraction obtained in Al-6Si-3.5Cu-Fe alloys. Additionally, strontium decrease the precipitation temperature of β-Al_5FeSi phase in Al-Si alloys [23]. Liu et al. [24] found that strontium have a poisining effect on the β-Al_5FeSi phase nucleation sites which results in a decrease of number of β-Al_5FeSi phase formed. The cooling rate can also influence the type and size of intermetallic phases formed during solidification [25].

1.2.2 Grain refinement

Smaller and more globular crystals formed during solidification of aluminium alloys enhance feeding, promote a finer and more uniform distribution of intermetallic phases and porosity and uniformity of mechanical properties [26–28]. Inoculation of aluminium alloys is the most common method to promote the formation of a fine, equiaxed microstructure [27].

Al-Ti-B master alloys are the most common grain refiners used in aluminium alloys [29]. For cast Al-Si alloys, typically with silicon concentrations greater than 3 wt.%, such as Al-7Si-Mg alloys, the silicon poisoning can occur, reducing the efficiency of the Al-Ti-B grain refiner [30,31]. The Al-B type grain refiners showed better grain refinement efficiency for Al-Si alloys with silicon concentration greater than 4wt.% in comparison to Al-Ti-B grain refiners [29]. Combined additions of strontium and boron-rich master alloys can result in the formation of SrB_6 particles [32,33] and decrease of grain refinement efficiency of Al-B grain refiners [32].

Vigorous stirring or agitation of the melt while being cooled is typical in SSM processes to produce slurries with non-dendritic crystals [34–37]. Yang et al. [38] reported a loss of the grain refinement efficiency of the Al-5Ti-B grain refiner in an electromagnetic stirred A356 alloy. The New Rheocasting (NRC) is a SSM process in which a superheated alloy is poured into a chill cup to generate a copious nucleation of crystals [39]. Easton et al. [39] found that the grain refinement effect of Al-5Ti-1B decreases as the pouring temperature is reduced in the NRC process.

1.3 SEMI-SOLID CASTING

SSM casting processes are divided in two main routes, thixocasting and rheocasting [40]. In the thixocasting process a solid billet with a non-dendritic microstructure is heated to a semi-solid temperature and injected into the die-cavity. In the rheocasting process the liquid alloy is cooled while being sheared to produce a certain fraction of non-dendritic crystals dispersed in the liquid. Subsequently, the mixture is injected into the die-cavity [4]. The main advantages of rheocasting are that traditional die casting alloys and the scrap produced in-house can be used in the process [40].

There are several rheocasting processes developed to produce SSM castings such as Semi-Solid Rheocasting (SSR™) [34], RheoMetal™ [36] Gas-Induced Semi-Solid (GISS) [35], NRC [39], Swirled Enthalpy Exchange Device (SEED) [37] and cooling slope method [41]. The Rheometal™ process is a very effective process that produces high solid fraction slurries in short times [36].

1.3.1 RheoMetal™ process

In the RheoMetal™ process a solid alloy block is immersed into a superheated alloy while being stirred. The solid alloy bock is at lower temperature compared to the superheated liquid before immersion. After immersion, an enthalpy exchange occurs between the liquid and the rotating solid alloy block, so-called Enthalpy Exchange Material (EEM). In the end of the process a slurry with a certain solid fraction and enthalpy is formed [42]. Subsequently, the slurry is poured into the shot sleeve and injected into the die cavity [43]. Figure 2 shows the steps sequence of the RheoMetal™ process.
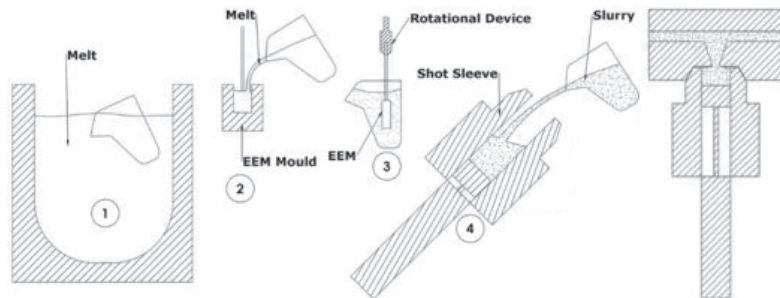
Figure 2: The RheoMetal™ process; 1) Alloy is collected from the furnace, 2) cast EEM 3) EEM is immersed into the superheated alloy while being stirred and 4) the slurry is poured into the shot sleeve and injected in the die-cavity [43].

The most critical process parameters in the Rheometal™ process are the alloy composition, liquid superheat, EEM stirring rate, EEM wt.% addition, EEM temperature and EEM microstructure [9,44]. Payandeh et al. [42,44] found that columnar α-Al dendrites grow on the EEM surface when is immersed into the liquid while being stirred, denoted freeze-on layer.

1.3.2 Microstructure

Hitchcock et al. [45] identified three different primary α-Al populations formed in SSM casting, shown in Figure 4 a). These α-Al populations are distinguished by their size and shape. The large α-Al globules, identified as α_1, are formed during the slurry preparation process under intensive shear forces. Subsequently, the slurry is poured into the relatively cold shot sleeve, where the smaller and dendritic α-Al identified as α_2 can form. In the die cavity, solidification occurs with the growth of α_1 and α_2-Al crystals, nucleation and growth of in-cavity solidified crystals and ends with the eutectic formation. The fine and globular in-cavity solidified α-Al are identified as α_3 in Figure 4 a).
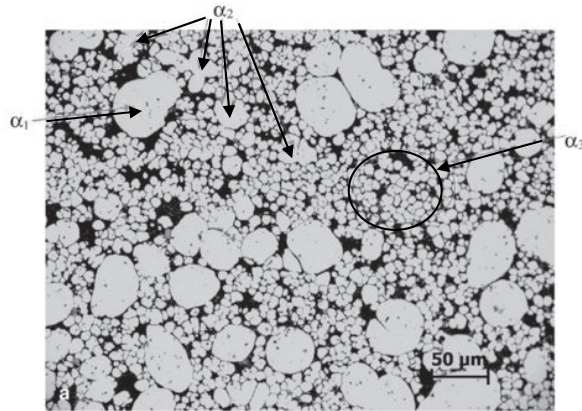
Figure 3: Microstructure obtained in an A357 rheocasting [45].

Payandeh et al. [43] measured the silicon concentration in the interior of the α_1-Al globules of quenched slurries for alloys with different silicon contents. The results showed that the silicon concentration in the interior of the α_1-Al was very uniform for all alloys, as shown in Figure 4. In the same work similar results were obtained for the α_1-Al in the SSM castings.
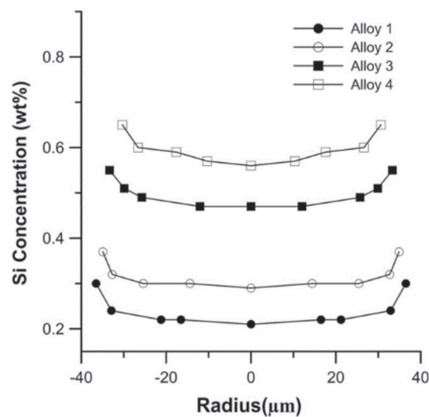
Figure 4: Silicon concentration profile over the diameter of the α_1-Al globules of Rheometal™ quenched slurries for different alloys [43].

1.3.3 Segregation

Surface segregation is a common feature of SSM castings [46] which involves a region at the casting surface, with a distinct microstructure and solute content compared to the centre of the casting [47]. This surface segregation strongly contributes to heterogeneous properties along the cross section of the casting [47]. Figure 5 a) shows the microstructure of an A357 SSM casting where the region near the casting

surface have a distinct microstructure compared to the centre, so-called surface segregation.

Dilatant shear bands can form in solidifying metals when sheared within a range of solid fractions [48]. Previous works proposed that the shear bands observed in HPDC [48,49] and SSM casting [50] result from localized deformation within the partially solidified material. These dilatant shear bands can take the form of porosity bands or positive macrosegregation when the shrinkage is adequately compensated [48,51]. Figure 5 b) shows a typical shear band in a low silicon SSM casting produced by the Rheometal™ process.
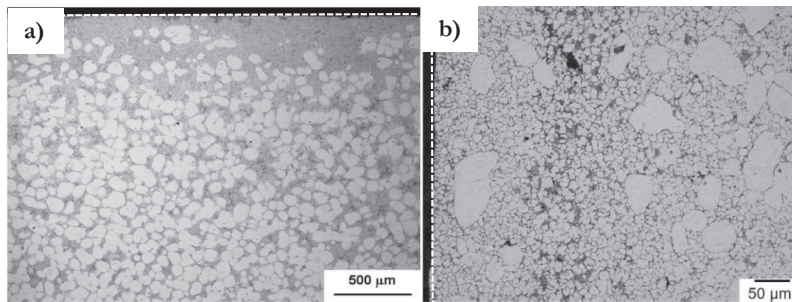
Figure 5: Micrographs obtained from SSM castings showing; a) Surface segregation [52] and b) shear band [50]. The dashed line shows the die wall position during casting.

1.3.4 Heat Treatment

The effectiveness of the T5 and T6 heat treatments is strongly affected by the level of magnesium supersaturation of the primary α-Al at the artificial aging temperature for Al-7Si-Mg alloys [53]. Increasing the supersaturation of magnesium in α-Al promotes the formation of a larger amount of metastable and coherent β'' precipitates and increases the hardening response of the Al-7Si-Mg alloys during aging [53].

In the T6 heat treatment, a solution treatment is applied to homogenise the primary α-Al, dissolve the Mg_2Si phase and reduce the fraction of π-$Al_8FeMg_3Si_6$ phase which transforms to β-Al_5FeSi, releasing magnesium into solution [14,54]. Möller et al. [53] studied the T6 heat treatment response of semi-solid processed A356 and F357 aluminium alloys. The results showed that for magnesium levels above 0.4wt.%, the π-$Al_8FeMg_3Si_6$ phase is just partially transformed into magnesium-free β-Al_5FeSi phase during solution treatment at 540°C [16]. This incomplete transformation reduces the maximum amount of magnesium that could be dissolved into α-Al and consequently reduced the achievable strength [14,55]. Similar results were reported in other studies for conventional casting processes [8,10].

The time at which the alloy remains in the semi-solid state is longer for SSM casting in comparison to conventional HPDC [13]. Therefore, the concentration of solute in the interior of the primary α-Al is more uniform in SSM castings compared to HPDC castings. This characteristic can result in shorter solution treatment times for the T6 heat treatment in SSM castings [13].

6

The T5 heat treatment is less expensive and distortion and blistering are prevented compared to T6 heat treatment [7,13]. However, the strength obtained for castings after T5 heat treatment is generally significantly lower compared to castings after T6 heat treatment [56,57].

1.4 KNOWLEDGE GAP

From the literature review, most of the existing knowledge of grain refinement, segregation and heat treatment response is mainly related to other casting processes, such as HPDC. However, SSM castings start to be used in applications where HPDC castings are not typically used, such as thick-wall castings. Therefore, there is a great need for a better understanding of SSM castings microstructure, segregation and defect formation. Additionally, mechanical properties data obtained for different heat treatments conditions is relevant for industry to design SSM castings.

The formation of globular and smaller crystals during slurry preparation can improve feeding, promotes a more uniform dispersion of porosity and intermetallic phases and increase of fatigue resistance [58,59]. The effect of stirring on grain refinement effectiveness is still not clear from literature. Therefore, the effect of grain refinement on α_1-Al crystals formed during slurry preparation and on the final microstructure is studied in this work.

Several studies are found regarding the effect of magnesium on heat treatment response, however, most of them focus on the T6 heat treatment. The T5 heat treatment is less expensive and blistering is prevented compared to the T6 heat treatment. Therefore, the effect of magnesium on T5 heat treatment response is relevant to increase the hardening response during artificial aging.

RESEARCH APPROACH

CHAPTER INTRODUCTION

This chapter introduces the purpose and aim of the study and describes the experimental procedure.

2.1 PURPOSE AND AIM

The purpose of this work is to analyse the effect of grain refinement, magnesium content and heat treatment on microstructure and mechanical properties of Al-7Si-Mg semi-solid castings.

The aim is to increase the knowledge on slurry and microstructure formation and heat treatment response of SSM castings.

2.2 RESEARCH DESIGN

2.2.1 Research perspective

In this work, independent variables are intended to be manipulated to study a response. Therefore, experimental design method is the most suitable for this study.

The research topic was identified considering industrial needs. Subsequently, literature review reveals the knowledge gaps within the topic and research questions were formulated. A series of experiments based in the research questions were designed and executed. Through data collection and analysis, conclusions can be stated.

2.2.2 Research questions

The current study pretends to improve the existing knowledge on slurry and microstructure formation and mechanical properties of SSM castings. Consequently, this study tries to answer the following research questions:

1. What is the influence of grain refinement on α_1-Al globules formed during Rheometal™ slurry preparation process? (Supplement I)

The grain refinement is a common practice of the foundries in aluminium casting. However, few studies are found relative to the effect of grain refinement in SSM casting.

2. What is the effect of magnesium and heat treatment on the mechanical properties of Al-7Si-Mg semi-solid castings? (Supplement II)

The relation of magnesium solubility in α_1-Al phase with the effectiveness of the T5 and T6 heat treatments response is intended to be clarified.

3. What is the effect of the die temperature and wt.% EEM addition on the defect formation of thick-walled Al-7Si-Mg semi-solid castings? (Supplement III)

The influence of the different parameters of the SSM casting process in the defect formation is addressed in this question.

2.2.3 Overview of the study

Experiments were designed and executed to address the research questions. Therefore, the work was divided in three stages listed below:

- The influence of grain refinement on the α_1-Al grain size, shape factor and solid fraction was studied in Supplement I. Additionally the solute content of the surface segregation layer was analysed.

- The effect of magnesium on the formation of intermetallics and the heat treatment response was evaluated in Supplement II. Identification of the intermetallic phases formed during solidification and the mechanical properties were correlated to the magnesium and silicon concentration in the interior of the α_1-Al.

- In Supplement III the effect of the die temperature and EEM wt.% addition on segregation bands and defects formation of aluminium SSM castings was investigated.

2.3 MATERIALS AND EXPERIMENTAL PROCEDURE

2.3.1 Alloys

Pre-modified commercial base alloys ingots from Salzburger Aluminium Group (SAG), Al-7Si-0.3Mg and Al-7Si-0.45Mg were used in this work. To produce an Al-7Si-0.6Mg alloy, pure magnesium was added to the Al-7Si-0.45Mg to obtain the intended magnesium content in the alloy after melting.

A Hindenlang SLEPM electrical resistance furnace was used for melting the alloys. The chemical composition of the alloys was measured by an optical emission spectroscopy Spectromaxx LMX06. Samples of the liquid alloy were collected from the furnace and quenched in a steel mould to produce discs for chemical analysis. Before the first measurement, chemical analysis on standard samples with a known composition was conducted. At least five measurements were performed in each sample.

The compositions range of the Al-7Si-0.3Mg alloy used in this study is shown in Table 1. For the alloys Al-7Si-0.45Mg and Al-7Si-0.6Mg a single melt was produced and the average composition in shown in Table 1.

Table 1: Chemical composition measured of the Al-7Si-Mg alloys used to produce the SSM castings. Compositions in wt.%.

Alloys	Si	Fe	Cu	Mg	Ti	Al
Al-7Si-0.3Mg	6.85-7.10	0.11-0.16	0.011-0.072	0.26-0.35	0.07-0.15	Bal.
Al-7Si-0.45Mg	7.24	0.11	0.021	0.47	0.11	Bal.
Al-7Si-0.6Mg	6.94	0.12	0.014	0.59	0.11	Bal.

To study the effect of grain refinement in SSM casting, Al-7Si-0.3Mg alloy melts were prepared, one with the base alloy, one with the addition of 0.15wt.% of Al-8B tablet and another with the addition of 0.20wt.% of Al-5Ti-1B master alloy rod. The master alloy rod and tablet were wrapped in aluminium foil, preheated to 200°C and immersed into the liquid held at 700±10°C. 15min after addition, the liquid was stirred for homogenization.

2.3.2 Semi-Solid Casting

The Rheometal™ [9] process was used to produce semi-solid castings from the different alloys in Table 1. For the slurry preparation, Enthalpy Exchange Material (EEM) was cast from the alloys in a copper die with a 40mm diameter cylindrical cavity and internal water cooling channels. A 12mm diameter stainless steel rod was inserted along the copper die cavity centre line to be cast in the EEM interior. After casting, EEM excess was cut off to ensure an addition of 7% of the total shot weight. The rod and EEM, preheated to 200°C, were inserted into a stirring device a few seconds before immersion into the liquid. Around 1.3kg of superheated liquid aluminium alloy was ladled from the furnace. As the temperature reached 650°C (~35°C superheat), the preheated EEM was immersed into the liquid while rotating at 850rpm. When the turbulence on the surface stopped, the slurry preparation process was assumed to be complete. The time for slurry preparation was approximately 18s.

The prepared slurry, primary α_1-Al crystals surrounded by liquid, was poured into the shot sleeve of a 50 tonne Vertical High Pressure Die Casting (VHPDC) machine to produce the casting as shown in Figure 6 a). The machine parameters were kept constant in all experiments with the plunger advance speed of ~0.3m/s and an intensification pressure of 160bar. The die temperature was controlled by internal oil circulation set at 175°C, using a PolyTemp HTF 300 heater. To maintain reproducible thermal conditions in the shot sleeve and die cavity, a first set of shots were performed before experiments started, to warm up the assembly. The relevant dimensions of the cast tensile bar are shown in Figure 6 b). This procedure was followed to produce the SSM castings for Supplements I and II.
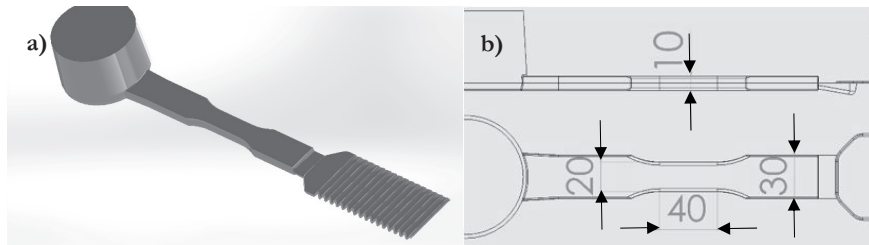
Figure 6: a) Casting shape and b) cast tensile bar dimensions in mm.

In supplement III, semi-solid castings, as shown in Figure 6 a), were produced with EEM additions of 6, 7, 8 and 9wt.%. For the different EEM additions, the die temperature was changed by set 175 and 240°C for the oil that circulates in the internal cooling channels of the die. For each condition, the plunger advance that forces the slurry into the die-cavity was stopped at three different positions. The goal was to study the die-cavity filling behaviour under the different conditions. The plunger positions were controlled by three 12mm diameter steel rods fixed to the plunger base, as shown in Figure 7. When the plunger advances to inject the slurry into the die-cavity, the rods follow the movement until their top hits the shot sleeve base. At this moment the movement is stopped, and the plunger position is preserved. Three different rod lengths were used to stop the filling front at different lengths inside the die-cavity.
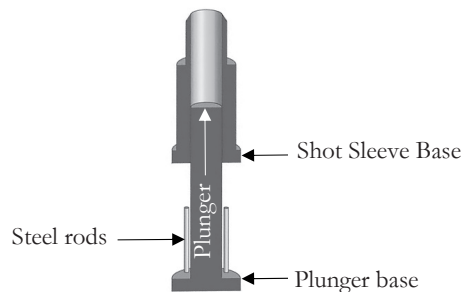
Figure 7: Illustration of the simplified VHPDC injection system. The white arrow shows the plunger movement direction.

2.3.3 Heat treatment

Heat treatments were applied to aluminium SSM castings to study their effect in the microstructure and mechanical properties in Supplement II. The T6 heat treatment consisted in a solution treatment using a Nabertherm L40/11 muffle furnace followed by quenching in water at room temperature. Within a period of 24h after quenching, the tensile bars were artificial aged using a Nabertherm TR-120 oven with air circulation followed by cooling in still air. The artificial aging treatment started within a period of 24h after casting for the case of T5 heat treatments.

The temperatures and holding times used for the heat treatments for each casting condition are shown in Table 2. The holding time in this work is the time that the tensile bars were kept at the solution and artificial aging temperatures. The temperatures and times used for the heat treatments in this work are based on a previous heat treatment optimisation study.

Table 2: Heat treatment temperatures and holding times used for the different Al-7Si-Mg alloys.

Alloy	Condition	Designation	Heat Treatment
Al-7Si-0.3Mg	T5	0.3Mg – T5	175°C/4.5h
Al-7Si.0.45Mg	T5	0.45Mg - T5	
Al-7Si-0.6Mg	T5	0.6Mg – T5	180°C/4.5h
Al-7Si-0.3Mg	T6	0.3Mg – T6	510°C/4h + 190°C/2h
Al-7Si-0.45Mg	T6	0.45Mg – T6	

2.4 CHARACTERISATION
2.4.1 Optical Microscopy

The cast tensile test bars were sectioned longitudinally along its midplane and studied by metallography, as shown in Figure 8 (supplements I, II and III). In supplement I the microstructural analysis focuses in the section B while for supplement II and III all sections were analysed. The samples for optical microscopy were ground and the last step of polishing was completed with 1μm diamond suspension. A 10%NaOH solution was used to etch the sample surface before microscopy in an Olympus GX71F.

A	B	C
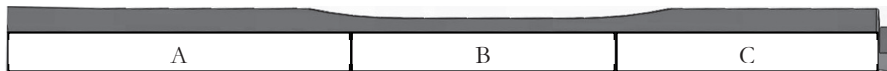
Figure 8: Section view of the cast tensile bar with the longitudinal cross-section investigated highlighted.

2.4.2 Solid fraction - Weck´s reagent

The manual point count method described in ASTM E562-11 [60] was used for the measurements of solid fraction on micrographs obtained from polished surfaces etched with Weck´s reagent. The Weck´s reagent was prepared with 4g $KMnO_4$, 1g NaOH and 100ml distilled water. A drop counter was used to release drops of reagent on sample surface. When the sample surface was totally covered by the Weck´s reagent and after a contact time of 12s, the reagent was immediately swept away using distilled water.

Solidification occur on existing solid during quenching from a semi-solid temperature. If the quenching is fast enough, the segregation of solute elements in

the α_1-Al globules can be preserved. The segregation of solute elements, like titanium and silicon, in the α_1-Al globules is revealed by the different britnesses of the brown colour under the optical microscope in surfaces etched with Weck´s reagent. Therefore, the periphery regions of the α_1-Al globules, where the silicon segregate,s have a brighter colour while the α_1-Al globules core with smaller concentration of silicon is darker when observed in optical microscope [61].

Hu et al. [3] and Gao et al. [62] used Weck´s reagent to identify the growth layer formed during quenching on α_1-Al globules of SSM castings. In this work, the peripheral brighter regions in the α_1-Al globules observed in micrographs taken from surfaces etched with Weck´s reagent are assumed to have formed during solidification in the die-cavity. Consequently, the darker core is representative of the crystal size in the slurry before injection into the die-cavity.

2.4.3 Energy-Dispersive X-ray Spectroscopy (EDS)

For Scanning Electron Microscopy (SEM) a last step of polishing with OP-U suspension was performed and the samples were observed unetched. The silicon content in the surface segregation layer was measured by EDS in a JEOL 7001F SEM for comparison between unrefined and refined alloys (Supplement I). The measurement was performed in ten different regions of the segregation layer in each sample.

EDS compositional maps were used to identify iron intermetallic phases in castings in the as-cast and heat-treated condition in Supplement II. All measurements were performed with a fixed acceleration voltage of 15kV.

2.4.4 Electron Backscattered Diffraction (EBSD)

EBSD analysis was performed in a JEOL JSM-7001F SEM operated at 20kV with a step size of 5µm to identify the α-Al grains (grain boundaries >15°) and Low Angle Grain Boundaries (LAGB) (grain boundaries between 0-15°). The EBSD analyses were performed in the centre of the cross-sections, where the Externally Solidified Crystals (ESCs) migrate during die filling [63]. The goal was to analyse the α_1-Al grains formed during slurry preparation in Supplement I. An image analysis software was used to determine grain size and shape factor of the grains identified with EBSD. At least 150 grains were analysed in each sample.

2.4.5 Wavelength-Dispersive Spectroscopy (WDS)

Silicon and magnesium contents were measured in the interior of α_1-Al globules using WDS in Supplement II. The measurements were made in the centre of the α_1-Al globules in an area of 225µm2. A minimum of 5 globules were analysed in each sample. The acceleration voltage was set to 10kV and pure elements were used as standards.

2.5 DIFFERENTIAL SCANNING CALORIMETRY (DSC)

DSC analysis was performed in a Netzsch 404 DSC. A sapphire disc was used as reference material. Baselines were obtained by DSC measurements in empty crucibles. 5mm diameter cylinders were machined from the centre of the tensile bars in different conditions using a lathe and cut in height with a precision cut-off machine to obtain discs with a mass of 42±2mg. The discs for DSC analysis from each casting condition were inserted into a platinum-rhodium crucible coated with Al_2O_3. The crucible + disc was heated to 660°C at a rate of 10k/min, held for 5min, and then cooled to 40°C at the same rate. This is called the first heating cycle. As the temperature reached 40°C, the samples were held for 15min and then the previously cycle was repeated. This is called the second heating cycle. During the DSC analysis, argon flowed through the system at a rate of 20ml/min to minimize oxidation. Three samples were tested for each condition. The characteristic temperatures were determined from the first derivative (dT/dt).

2.6 TENSILE TESTING

Tensile testing was performed according to SS-EN ISO 6892-1:2016 [64] in samples as shown in Figure 6 b). No surface treatment or machining were performed in the castings before testing. A Zwick/Roell Z100 equipped with a 100KN load cell was used for testing. A constant strain rate of $0.00025s^{-1}$ was set for yield strength determination and $0.002 \ s^{-1}$ further until sample fracture. A laser extensometer Zwick/Roell LaserXtens was used to record the elongation during the test. The tensile tests were performed in 5 samples for each condition in Supplement II.

CHAPTER 3

SUMMARY OF RESULTS AND DISCUSSION

CHAPTER INTRODUCTION

In this chapter, the main results of the appended papers are summarised and discussed.

3.1 MICROSTRUCTURE CHARACTERIZATION
3.1.1 Primary α_1-Al grain size

The effect of grain refinement on the α_1-Al grains size and shape in RheoMetal™ cast samples was investigated. One base alloy Al-7Si-0.3Mg and two grain refined alloys with Al-8B and Al-5Ti-1B were used to produce the castings. EBDS maps where individual α-Al grains are distinguished by different colours according to their crystallographic orientations are shown in Figure 9.
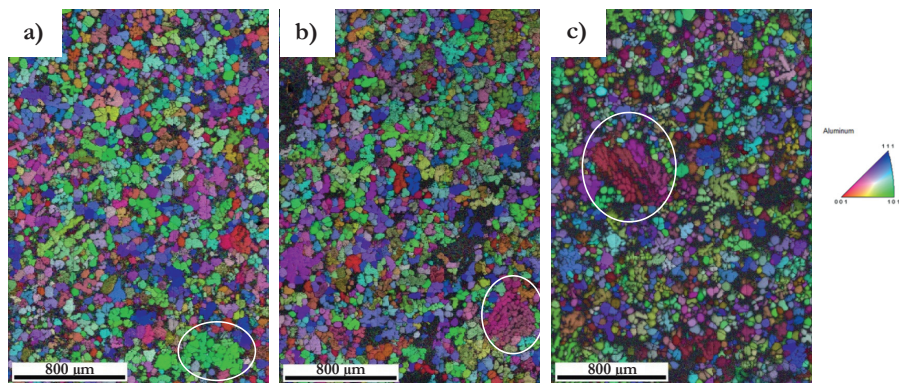
Figure 9: EBSD maps where individual grains are distinguished by different colours according to their crystallographic orientations; a) Base, b) base + Al-8B, and c) base + Al-5Ti-1B alloys.

Large dendrites were observed in all castings, as shown in Figure 9 highlighted by circles. These are likely α-Al grains formed in the shot sleeve or on the EEM surface during slurry preparation. Few crystals are formed in the shot sleeve during SSM casting and they are generally dendritic in shape and smaller than the α1-Al crystals formed during slurry preparation [43,45]. Payandeh et al. [42] reported the formation of long and bent columnar dendrites on the EEMs surfaces quenched after immersion into the superheated alloy while being stirred. The initial shape and size

of these columnar dendrites can change during the slurry preparation process and cavity filling. Therefore, the large dendrites observed in Figure 9 likely originate from the freeze-on layer.

The average equivalent circular diameter and shape factor were determined for all castings and the results are shown in Table 3. Grains with an average equivalent circular diameter smaller than 25μm and bigger than 190μm were removed from the results because grain refinement likely is not determinant for these grains size populations. Similar grains size and shape factors were obtained in all castings as shown in Table 3. Therefore, it seems that grain refinement has no significant effect in the RheoMetal™ process. However, other studies reported that grain refinement decreased the size and increase the sphericity of grains in SSM casting [65,66].

When the EEM at ~200°C is immersed into the liquid at 650°C while being stirred, a thermal undercooled region is stablished in the liquid close to the EEM surface. In this region, a copious crystal nucleation events can occur, similar to the "free chill crystal" nucleation mechanism suggested by Chalmers [67]. The continuous EEM stirring can homogenise the temperature and composition in the original liquid which promotes the survival of crystals [68,69]. It is possible that under these conditions, the grain refiner particles distributed in the liquid are not determinant in the nucleation of crystals. Crystals that are not attached to the EEM surface can be swept out of the thermal undercooled zone into the original bulk liquid flow by the rotation speed of the EEM. The crystals that are attached to the EEM surface grow as columnar dendrites into the original liquid, so-called freeze-on layer [42]. Fragmentation of the columnar dendrites formed on the EEM surface can occur because of the stirring rate and additional crystals can be added into the liquid that are not affected by the grain refiner particles in the liquid. The initial thermal undercooling near EEM and dendrite fragments originated from the freeze-on layer may decrease the effect of the nucleant particles in the liquid. The disintegration of EEM can result in additional crystals added to the original liquid [42], which are also unlikely affected by the grain refiner particles in the liquid.

Table 3: The average equivalent circular diameter and shape factor obtained for each casting.

Castings	Average equivalent circular diameter (μm)	Shape factor
Base alloy	72±19	0.44±0.15
Base + Al-8B	73±18	0.46±0.16
Base + Al-5Ti-1B	71±17	0.43±0.17

3.1.2 Primary α_1-Al solid fraction

The solidification in the Rheometal™ slurry preparation process starts with the formation of the primary α_1-Al crystals. When the slurry preparation process is complete, a mixture of α_1-Al crystals dispersed in a solute enriched liquid is poured into the shot sleeve. Solidification likely occurs in the shot sleeve at some extent because of its relatively low temperature. However, in the shot sleeve, particularly for the VHPDC used in this study, the solidification most likely occurs mainly at the

bottom, where the slurry is in contact with the piston, which is cooled by internal water cooling channels. Solidification can also occur close to the shot sleeve walls, but at much lower extent. When the piston advances vertically and forces the slurry into the die-cavity, most of the α_2-Al crystals formed in the shot sleeve, likely remain in the large biscuit section of the casting, Figure 6 a). Therefore, in the die-cavity, solidification occurs mostly with the growth of α_1-Al crystals from the slurry, nucleation and growth of in-cavity solidified crystals and ends with the formation of eutectic.

The effect of grain refinement on the α_1-Al globules fraction in SSM castings was investigated. Figure 10 a) shows a representative microstructure of the SSM casting refined with Al-8B and etched using Weck's reagent. The α_1-Al globules have a dark brown core and a brighter peripheral layer. As referred previously in 2.4.2, the brighter peripheral layer is assumed to have formed during solidification of the α_1-Al crystals in the die-cavity while the darker core is representative of the crystal area before slurry injection into the die-cavity. Therefore, the area fraction obtained for the darker core is assumed to be the slurry solid fraction before injection. Additionally, when both the brighter peripheral layer and darker core are included, the area fraction obtained is not a solid fraction but the α_1-Al globule fraction when the solidification is complete in the die-cavity. Figure 10 b) shows that for the alloy refined with Al-5Ti-1B was obtained lower solid fraction compared to the refined with Al-8B and unrefined alloys. Similar solid fraction was obtained for both unrefined and refined with Al-8B alloys. However, when the solidification is completed the unrefined alloy shows a significant larger α_1-Al fraction compared to both refined alloys.
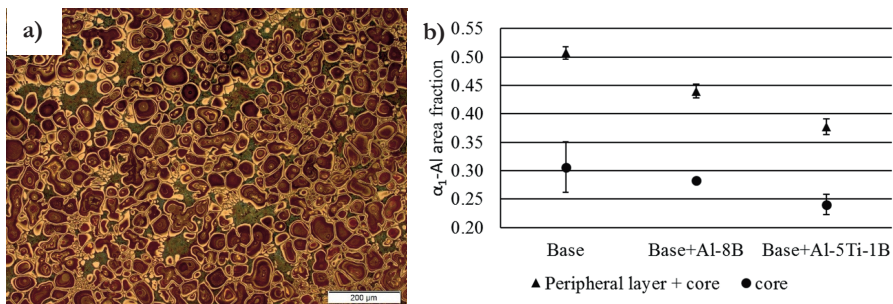
Figure 10: a) Micrograph of the casting refined with Al-8B etched with Weck's reagent showing α-Al globules with a dark brown core surrounded by a brighter periphery, b) α-Al area fraction considering the brighter periphery + core and darker core, as observed in Figure 10 a).

The α_1-Al globules fraction increased 20, 16 and 14% during solidification in the die cavity for the unrefined and refined with Al-8B and Al-5Ti-1B alloys, respectively. Therefore, the α_1-Al globules growth during solidification in the die-cavity was inferior for the refined alloys, as shown in Figure 10 b).

Titanium is a solute element with a large growth restriction factor [26]. The alloy refined with Al-5Ti-1B contained higher titanium content in its composition in

comparison to the unrefined and refined with Al-8B alloys. Therefore, the smaller growth obtained for the α_1-Al globules of the alloy refined with Al-5Ti-1B during solidification in the die cavity may be explained by its greater titanium content. However, it would be expected that this larger growth restriction for the alloy refined with Al-5Ti-1B would decrease the grain size, which was not verified as shown in Table 3.

Table 4 shows the silicon concentrations measured in the interior of the α_1-Al globules by WDS for all alloys. These silicon concentrations were used to calculate the corresponding solidus temperatures in Thermocalc™ for each alloy, shown in Table 4. The solidus temperature was used to calculate the corresponding solid fraction in Thermocalc™, shown in Table 4. The solid fraction calculated in Thermocalc™ was inferior for all alloys in comparison to the determined from micrographs of etched surfaces, Table 4 and Figure 10 b) respectively.

Table 4: Silicon concentration (wt.%) measured in the interior of the α_1-Al globules and the corresponding slurry temperature (°C) and solid fraction calculated in Thermocalc™ for each alloy.

Alloy	Silicon concentration	Thermocalc™	
		Slurry temperature	Solid fraction
Base	0.99±0.04	602	0.23
Base + Al-8B	1.00±0.04	602	0.22
Base + Al-5Ti-1B	0.94±0.03	605	0.20

3.1.3 Misorientation angles distribution of α-Al grain boundaries

The misorientation angles distribution of grain boundaries for the refined and unrefined castings are shown in Figure 11. The eutectic regions were removed from the results by setting a minimum grain size of 10μm and a minimum Confidence Interval (CI) of 0.1. The misorientation angles distribution in the interval from 5 to 50 degrees is similar for all castings. However, between 50 to 60 degrees both the refined castings show higher number fraction of grain boundaries compared to the unrefined alloy. Additionally, both refined alloys have a similar evolution of boundaries angle distribution in the range of 50 to 60 degrees of misorientation. The α-Al grain boundaries that surround the eutectic regions have very low CI, similar to the eutectic regions. Therefore, these grain boundaries are not included in the results, which may influence the distribution shown in Figure 11.
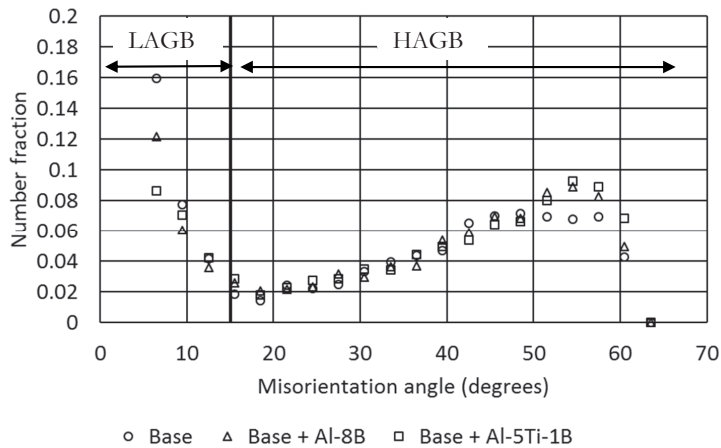
Figure 11: Misorientation angles distribution of grain boundaries.

Liquid penetration in primary α-Al. Crystals bending can occur during HPDC by mechanical stresses, particularly in branched dendrites [70]. Doherty et al. [71] showed that High Angle Grain Boundaries (HAGB) can form in bent crystals of aluminium at high temperature. The misorientation angles between adjacent regions in the interior of the crystals becomes larger as deformation increases. When a misorientation exceeds ~15° a HAGB is formed and liquid wetting at the grain boundary can occur. This occurs because the interfacial energy at grain boundaries (y_{gb}) becomes superior to the solid-liquid interfacial energy ($y_{s/l}$), $y_{gb} > y_{s/l}$, and liquid wetting at grain boundary occurs [70]. Subsequently, the disintegration of the crystal by liquid penetration can occur, as observed by Karagadde [72].

Gao et al. [61] reported that Weck´s reagent can reveal HAGB in the interior of α-Al globules. Figure 12 shows a representative microstructure obtained from the unrefined alloy etched with Weck´s reagent. One region of the micrograph shown in Figure 12 is highlighted where it is observed what seems to be liquid wetting at a HAGB, region 1, and black lines in the interior of an α_1-Al globule that may be HAGB as reported by Gao et al. [61]. This suggest that crystals deformation and liquid wetting at HAGB can occur during the Rheometal™ process. It is likely that this occur during intensification pressure stage, where the crystals are more densely packed and larger stresses are transmitted. In these conditions, formation of HAGB in deformed crystals can occur, particularly in branched crystals as the grain highlighted in Figure 12, followed by liquid wetting and disintegration of the crystal.
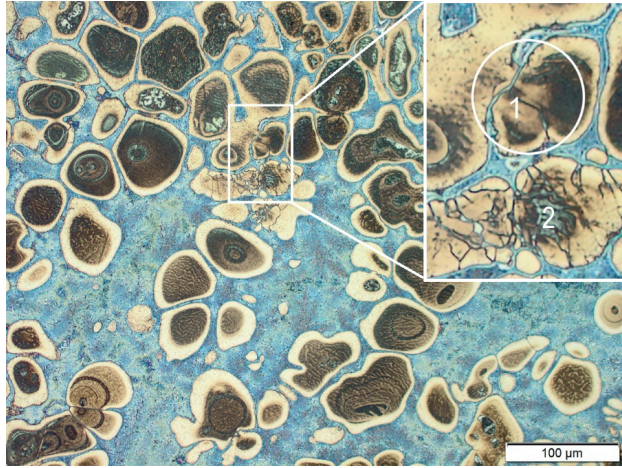
Figure 12: Micrograph from the Al-7Si-0.3Mg unrefined casting showing liquid penetration (region 1) and possible HAGB revealed by Weck´s reagent (region 2).

3.1.4 Silicon and magnesium concentrations in the interior of α_1-Al globules

The silicon and magnesium concentrations measured in the interior of the α_1-Al globules of the different castings are shown in Figure 13. Excluding the Al-7Si-0.45Mg casting in the T5 condition, the silicon concentration in the interior of the α_1-Al globules is similar for all castings. The Al-7Si-0.45Mg have a slighter higher concentration of silicon in the interior of the α_1-Al globules compared to the other castings. However, the magnesium concentrations in the interior of the α_1-Al globules shows a different result compared to the silicon concentration. The magnesium concentration in the interior of the α_1-Al globules increases with the increase of magnesium content of the alloy, for the castings in the T5 and T6 conditions, as seen in Figure 13. Additionally, the alloys in the T6 condition show a significant higher concentration of magnesium in the interior of the α_1-Al globules in comparison to the same alloys in the T5 condition. However, the concentrations obtained for the Al-7Si-0.3Mg and Al-7Si-0.45Mg castings in the T6 condition, 0.23 and 0.37wt.% respectively are lower than the magnesium content of the alloy. This indicates that magnesium is partly bind into the intermetallic phases.

The magnesium concentration in the interior of the α_1-Al globules of the Al-7Si-0.3Mg castings in the T5 condition is too low to have a substantial precipitation hardening effect during aging compared to the T6 condition. Sjölander and Seifeddine [12] measured concentrations of 0.04 and 0.1wt.% magnesium in the interior of α-Al dendrites of directionally solidified castings with SDAS of 10 and 51, respectively. Pedersen and Arnberg [73] obtained 0.05 and 0.1wt.% magnesium for an Al-7Si-0.24Mg direct chill casting with SDAS of 13 and 52μm, respectively. Therefore, it seems that the magnesium concentration in the interior of α-Al dendrites increases as the cooling rate decreases.

22
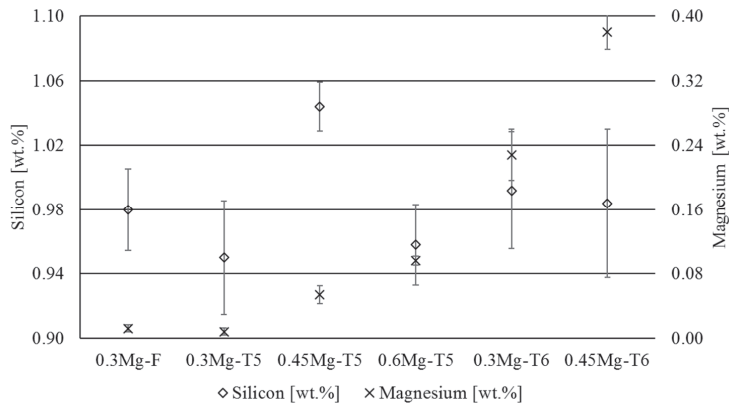
Figure 13: Silicon and magnesium concentrations measured in the interior of the α_1-Al globules for the different castings.

Figure 14 shows the solidus lines for silicon and magnesium calculated in Thermocalc™ for the Al-Mg-Si system at different temperatures in the solidification range. The solidus lines show that the magnesium solubility in α-Al depends on silicon concentration. The magnesium concentration measured in the interior of the α_1-Al globules, the solidus lines shown in Figure 14 and the literature [12,73] suggest that the magnesium solubility in α-Al at temperatures in the solidification range of the Al-7Si-Mg alloys is very low.

Figure 14: Solidus line of the primary α-Al phase in the Al-Mg-Si system at different temperatures [18].

3.1.5 Intermetallic phases

The influence of magnesium on the intermetallic phases formed in Al-7Si-Mg cast alloys was studied. The intermetallic phases that commonly form during

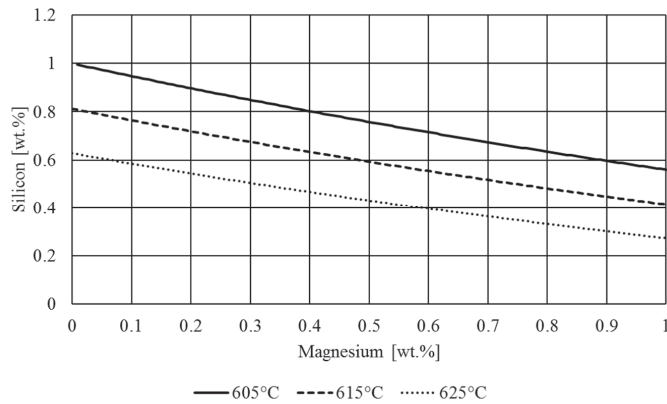solidification in these alloys are the β-Al$_5$FeSi, π-Al$_8$FeMg$_3$Si$_6$ and Mg$_2$Si phases [8,10]. Figure 15 shows representative microstructures obtained for the SSM castings with magnesium contents of 0.3 and 0.45wt.% in the T5 and T6 conditions. The microstructure of all alloys after T5 heat treatment consisted of primary α-Al globules, modified Al-Si eutectic and a minor fraction of intermetallic phases distributed in the eutectic regions, as shown in Figure 15 a) and b). The as-cast Al-7Si-0.3Mg alloy microstructure was similar compared to at observed in Figure 15 a).

Figure 15 c) and d) show the microstructures obtained for the castings in the T6 condition which consisted of primary α-Al globules, coarse and spheroidised eutectic silicon and a minor fraction of intermetallic phases in the eutectic regions. Shorter and thinner intermetallic phase platelets are observed in the eutectic regions for the Al-7Si-0.3Mg casting in comparison to the Al-7Si-0.45Mg casting, as shown in Figure 15 c) and d).
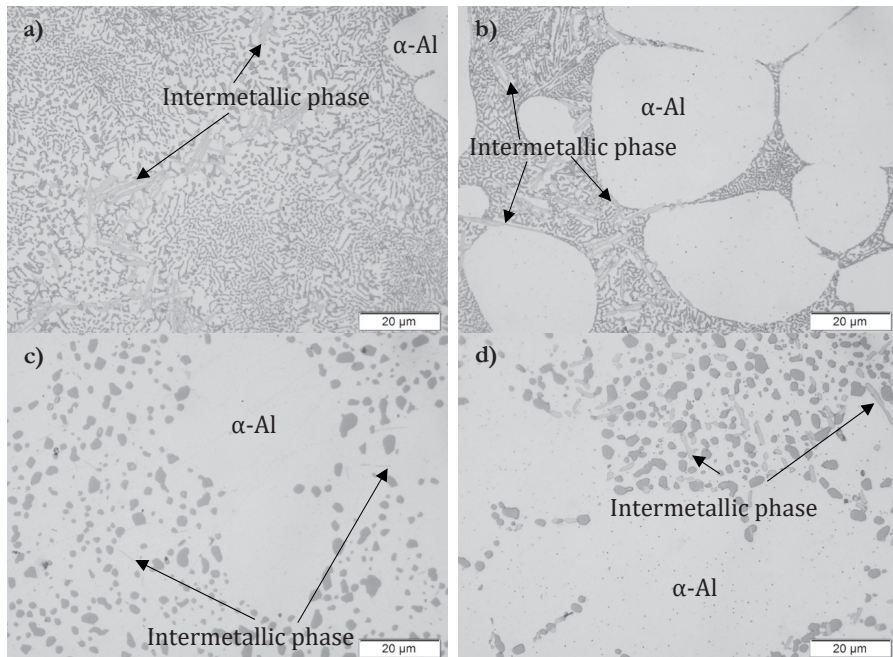
Figure 15: Micrographs obtained for each condition. Dark grey – Eutectic silicon. Light grey – iron-rich intermetallic phase. a) 0.3Mg – T5. b) 0.45Mg – T5. c) 0.3Mg - T6. d) 0.45Mg – T6.

The identification of the intermetallic phases obtained for the different castings was based on the analysis of the EDS maps, as shown in Figure 16, and literature [8,12,21]. Figure 16 shows SEM micrographs and the corresponding EDS maps of silicon, magnesium and iron. The π-Al$_8$FeMg$_3$Si$_6$ phase was the only intermetallic phase detected in the Al-7Si-0.3Mg casting in the T5 condition, as shown in Figure 16 a). The same phase was obtained for the Al-7Si-0.3Mg casting in the as-cast condition. In addition to the π-Al$_8$FeMg$_3$Si$_6$, Mg$_2$Si phase is observed in the eutectic regions when the magnesium content of the alloys is increased, as shown in Figure 16 e) for the Al-

7Si-0.45Mg casting in the T5 condition. The same intermetallic phases were obtained for the Al-7Si-0.6Mg casting compared to the Al-7Si-0.45Mg casting.

In the T6 condition, the intermetallic phase identified for the Al-7Si-0.3Mg casting was mostly β-Al_5FeSi, as the magnesium concentration was lower at the intermetallic region compared to the surroundings, as shown in Figure 16 e-h). This indicates that the π-$Al_8FeMg_3Si_6$ phase obtained in the as-cast condition transformed into β-Al_5FeSi phase and released magnesium into solid solution. For the Al-7Si-0.45Mg casting in the T6 condition, the π-$Al_8FeMg_3Si_6$ phase remains in the eutectic regions with a minor fraction of β-Al_5FeSi platelets observed on the π-$Al_8FeMg_3Si_6$ phase, as indicated in Figure 16 m).
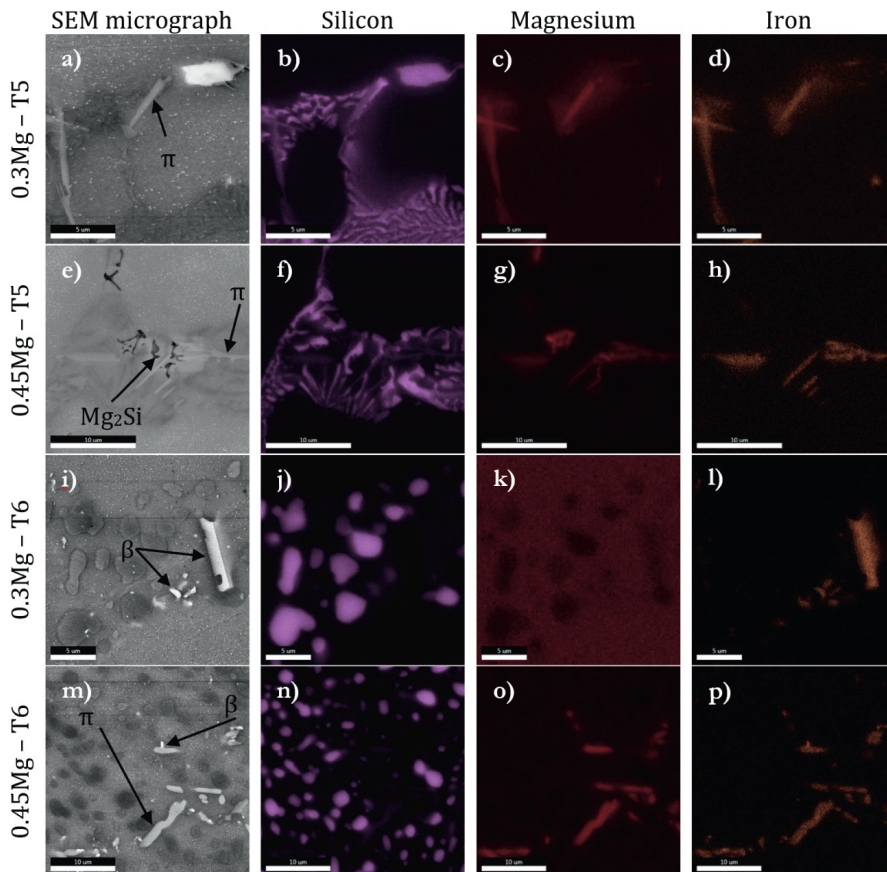
Figure 16: EDS maps showing the silicon, magnesium and iron distribution in the different castings. a-d) Al-7Si-0.3Mg-T5 (scale bar 5μm), e-h) 0.45Mg-T5 (scale bar 10μm), i-l) 0.3Mg-T6 (scale bar 5μm) and m-p) 0.45Mg-T6 (scale bar 10μm).

DSC was used to study the formation sequence of the intermetallic phases identified in Figure 16. Figure 17 a) and b) shows the DSC curves and characteristic temperatures obtained during the first and second heating cycles, respectively, for

each alloy in the T5 condition. In the beginning of the first heating cycle in the DSC, the samples have the original SSM casting microstructure, as seen in Figure 15. At the start of the second heating cycle the microstructure of the DSC sample was generated by the cooling rate in DSC. Therefore, the DSC heating curves shown in Figure 17 a) are identified with the alloy and initial condition of the casting while the heating curves in Figure 17 b) are identified just with the alloy. The characteristic temperatures shown in Figure 17 for the reaction II are not accurate because of the overlapping of adjacent peak reactions.

Two peak reactions are observed in the DSC curves for the Al-7Si-0.45Mg and Al-7Si-0.6Mg castings in the T5 condition, as observed in Figure 17 a). For the Al-7Si-0.3Mg casting only the peak reaction II was observed and consequently, this peak reaction most likely results from the dissolution of the π-$Al_8FeMg_3Si_6$ because was the only intermetallic phase identified in this casting. Consequently, the peak reaction I results most likely from the dissolution of Mg_2Si, that occurs at lower temperature compared to the π-$Al_8FeMg_3Si_6$.phase. The heat of reactions increases with the increasing of magnesium content of the alloy. This suggests that a larger volume fraction of intermetallic phases is formed during solidification of the alloys with higher magnesium content, as seen in Figure 17.
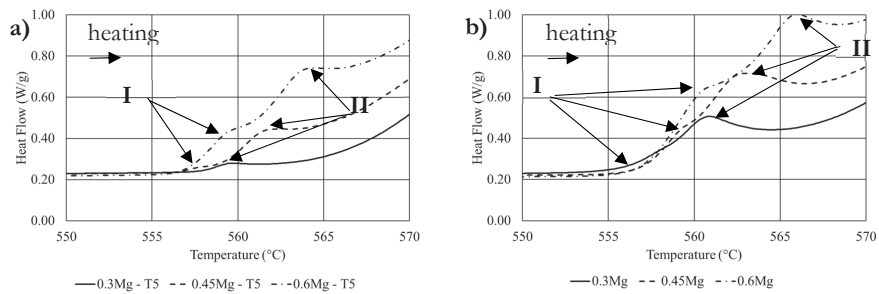
Reaction	Temperature (°C)			Reaction	Temperature (°C)		
	0.3Mg-T5	0.45Mg-T5	0.6Mg-T5		0.3Mg	0.45Mg	0.6Mg
I	---	555	554	I	552	553	553
II	556	558	560	II	558	560	562

Figure 17: DSC heating curves and characteristic temperatures obtained for each alloy in the T5 condition. a) first heating cycle, b) second heating cycle.

The microstructure of the Al-7Si-0.3Mg alloy after two heating/cooling cycles in the DSC is shown in Figure 18 a). The low cooling rate in the DSC change the original SSM microstructure significantly. Large eutectic silicon platelets are observed in addition to the intermetallic phases. The intermetallic phases observed in the Al-7Si-0.3Mg alloy after second heating/cooling cycle in the DSC were β-$Al5FeSi$ phase bound by π-$Al_8FeMg_3Si_6$ and Mg_2Si, as seen in Figure 17. The increase of heat flow for the Al-7Si-0.3Mg alloy starts at lower temperatures during the second heating cycle in the

DSC comparised to the first heating cycle, as seen in Figure 17 b) and a) respectively. This difference can be assumed that results from the Mg_2Si phase dissolution during the second heating cycle.
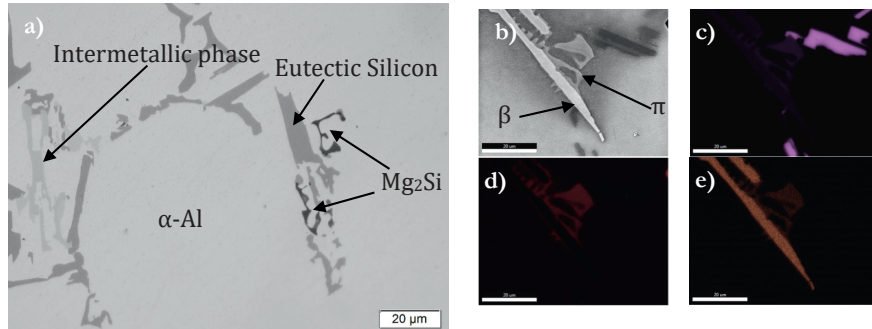

Figure 18: Micrograph of the Al-7Si-0.3Mg alloy after two heating/cooling cycles in DSC. a) Optical microscopy micrograph. Dark grey – Eutectic silicon. Bright grey – Intermetallic phase. Mg_2Si – Darker phase. b) SEM micrograph. EDS maps showing elements distribution obtained from region in b; c) silicon, d) magnesium and e) iron. The scale bar is 20µm.

Intermetallic phases formation during solidification. According to the phase diagram shown in Figure 1, the solidification of the alloys used in this study ends with the ternary eutectic reaction $L \Leftrightarrow Al + Si + \beta\text{-}Al_5FeSi$. However, in this work, the quaternary $\pi\text{-}Al_8FeMg_3Si_6$ phase was obtained instead of the $\beta\text{-}Al_5FeSi$ phase for all SSM castings in as-cast and T5 conditions, as seen in Figure 16. The $\pi\text{-}Al_8FeMg_3Si_6$ phase can be obtained during solidification through the peritectic reaction $L + \beta\text{-}Al_5FeSi \Leftrightarrow Al + Si + \pi\text{-}Al_8FeMg_3Si_6$ and the quaternary eutectic reaction $L \Leftrightarrow Al + Si + \pi\text{-}Al_8FeMg_3Si_6 + Mg_2Si$ [17]. Both reactions, occur for alloys with higher magnesium content than that investigated in this study, as shown in Figure 1. Therefore, the formation of $\pi\text{-}Al_8FeMg_3Si_6$ likely results from the non-equilibrium solidification that occurs in the die-cavity [17].

Low cooling rates generally favour the formation of $\beta\text{-}Al_5FeSi$ and at high cooling rates, the start temperature of $\beta\text{-}Al_5FeSi$ formation is decreased [25]. Consequently, the high cooling rate that occurs during solidification in the die-cavity, may decrease the $\beta\text{-}Al_5FeSi$ phase formation temperature to such an extent that the composition of the liquid favors the formation of the $\pi\text{-}Al_8FeMg_3Si_6$. The microstructural observations and the DSC heating curves analysis of this work suggest that $\pi\text{-}Al_8FeMg_3Si_6$ is formed instead of $\beta\text{-}Al_5FeSi$ during solidification of the SSM castings. The $\pi\text{-}Al_8FeMg_3Si_6$ is the only intermetallic phase observed in the eutectic regions of the Al-7Si-0.3Mg SSM castings, while for higher magnesium contents Mg_2Si is observed in addition to the $\pi\text{-}Al_8FeMg_3Si_6$. There is no evidence of $\beta\text{-}Al_5FeSi$ in the microstructure of the SSM castings, therefore, is unlikely that has formed by the peritectic reaction. Consequently, $\pi\text{-}Al_8FeMg_3Si_6$ most likely forms during the quaternary reaction $L \Leftrightarrow Al + Si + \pi\text{-}Al_8FeMg_3Si_6 + Mg_2Si$ in the SSM castings. This reaction may also occur for the lower magnesium casting Al-7Si-0.3Mg [21]. However, the volume fraction of Mg_2Si formed is likely too low to be observed in the microstructures and detected in the DSC heating curves. As the magnesium content of the alloy increases, larger fraction of $\pi\text{-}Al_8FeMg_3Si_6$ and Mg_2Si are formed as

suggested by the increase of the area under the peak reactions I and II, as seen in Figure 17 a).

As shown in Figure 18, β-Al_5FeSi, π-$Al_8FeMg_3Si_6$ and Mg_2Si phases are formed during solidification of the Al-7Si-0.3Mg alloy in the DSC. The π-$Al_8FeMg_3Si_6$ growing from the β-Al_5FeSi suggests that the peritectic reaction L + β-Al_5FeSi $\Leftrightarrow$ Al + Si + π-$Al_8FeMg_3Si_6$ occurs during the solidification in the DSC for this alloy. This also indicates that the ternary eutectic reaction L $\Leftrightarrow$ Al + Si + β-Al5FeSi has occurred previously to the peritectic reaction. The peritectic reaction was not completed during solidification in the DSC because the β-Al5FeSi phase is observed in the microstructure, as shown in Figure 18. The solidification in the DSC most likely ends with the quaternary eutectic formation, as both π-$Al_8FeMg_3Si_6$ and Mg_2Si were detected in the microstructure and in the DSC second heating curves, as shown in Figure 18 and Figure 17 b), respectively. The increase of magnesium content of the alloy result in larger fractions of Mg_2Si and π-$Al_8FeMg_3Si_6$ formed during solidification, as suggested by the increase of the area under the peak reactions I and II, Figure 17 b).

Dissolution of the intermetallic phases during solution treatment. Figure 19 shows the first heating curves in the DSC of the Al-7Si-0.3Mg and Al-7Si-0.45Mg alloys with the original SSM microstructure in the T6 condition. No peak reaction is observed for the Al-7Si-0.3Mg alloy during first heating in the DSC, suggesting that most of π-$Al_8FeMg_3Si_6$ has transformed into β-Al_5FeSi and released magnesium into α-Al solid solution. For the Al-7Si-0.45Mg casting in the T6 condition, a peak reaction is observed, likely result of π-$Al_8FeMg_3Si_6$ dissolution that remained in the microstructure after T6, as shown in Figure 19. Therefore, a fraction of magnesium of the alloy remains bound into the π-$Al_8FeMg_3Si_6$ phase after solution treatment.

Reaction	Temperature (°C)	
	0.3Mg-T6	0.45Mg-T6
I	---	---
II	---	559
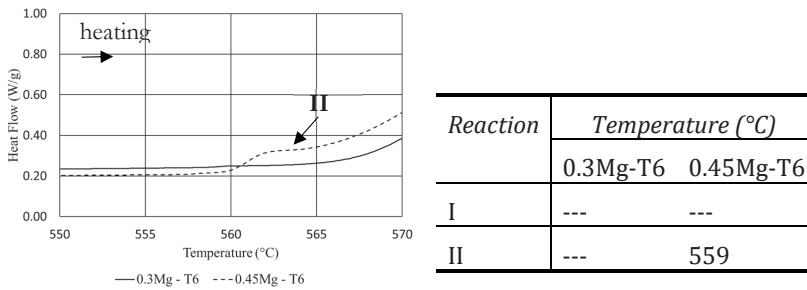
Figure 19: DSC heating curves and characteristic temperatures obtained for each alloy in the T6 condition.

According to the polythermal section of the Al-7Si-Mg-0.14Fe phase diagram shown in Figure 20, a fully transformation of π-$Al_8FeMg_3Si_6$ into β-Al_5FeSi and solution of all magnesium of the alloy into α-Al can occur for magnesium contents close to 0.45wt.%. However, in this study, the complete dissolution of the π-$Al_8FeMg_3Si_6$ phase was not achieved for the Al-7Si-0.45Mg. Similar results were reported in the literature for magnesium contents higher than 0.4wt.% [14].

Figure 20: Polythermal vertical section of the Al-7Si-Mg-0.14Fe phase diagram calculated in ThermoCalc™ [18]. The dashed lines show the composition range of the alloys studied in the T6 condition.

3.2 Segregation

Surface segregation. The influence of grain refinement on surface segregation was studied. Figure 21 shows the first 1mm surface layer near the die wall for the base (Al-7Si-0.3Mg) and refined alloys. A finer and more uniform microstructure is observed near the casting surface of the grain refined alloys, Figure 21 b) and c), compared to the unrefined alloy, Figure 21 a).

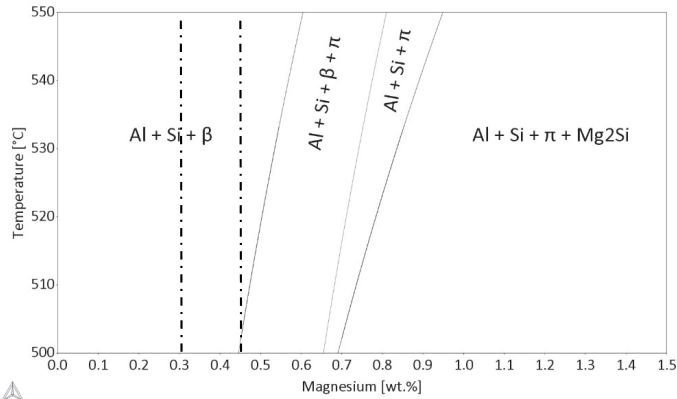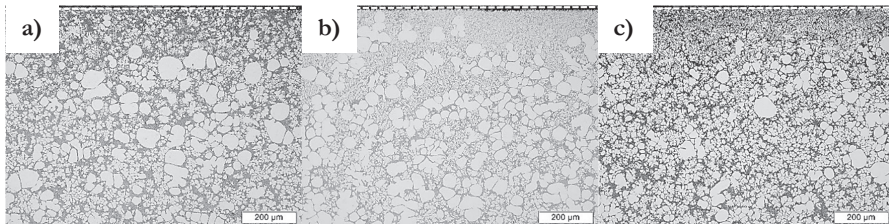Figure 21: Microstructures obtained near the castings surface for a) base (Al-7Si-0.3Mg); b) base + Al-8B; c) base + Al-5Ti-1B alloys. The top dashed line shows the die wall position during casting.

The silicon content of the α_1-Al interdendritic regions in the surface segregation layer was measured by EDS. The unrefined alloy showed higher silicon content in the surface segregation layer compared to the Al-5Ti-1B refined alloy. This is likely a consequence of the larger solid fraction obtained for the unrefined alloy, as shown in Figure 10 b), that results in more solute segregated to the liquid.

Segregation bands. The effect of EEM wt.% addition and die temperature on microstructure of SSM castings were analysed. Additionally, plunger advance movement was blocked at different lengths of die-cavity filling to analyse the

microstructure evolution of the solidified slurry during the die-cavity filling. The analysis of the quenched slurries during die-cavity filling (interrupted shots) showed that a planar front filling was obtained for all EEM wt.% additions and die temperatures used. The microstructure analysis of the quenched slurries in the die-cavity and SSM castings indicates that dilatant shear bands and V-shape bands formation occurs mostly during intensification pressure period, as suggested in literature [49].

Figure 22 a) shows a shear band formed close to the surface layer of the Al-7Si-0.3Mg cast at the higher die temperature. In this study, shear bands, as shown in Figure 22 a), were observed for EEM additions of 6 and 7wt.% when the higher die temperature was used. When the EEM additions was increased to 8 and 9wt.%, shear bands were not observed using both the higher and lower die temperatures. V-shape segregation bands were observed for all SSM castings. The SSM cast with EEM addition of 6wt.% using the lower or higher die temperatures showed formation of porosity in the interior of the V-shape band. Similar porosity bands were observed for the SSM cast with EEM addition of 7wt.% and using the higher die temperature, as seen in Figure 22 b). The formation of the V-shape segregation band may be related to the burst feeding mechanism. The burst feeding results from the collapse of the dendritic network formed in the casting and may occur in Al-Si cast alloys [74]. However, further investigation is necessary to understand the formation mechanism of the V-shape bands.

It seems that the formation of shear bands near casting surface can result in the formation of porosity in the interior of the V-shape bands, most likely shrinkage porosity.
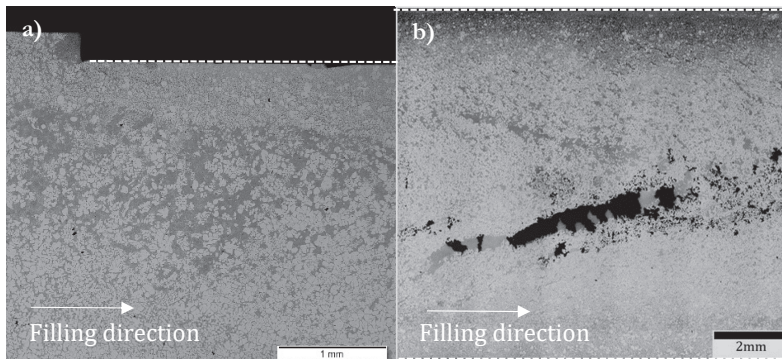
Figure 22: a) Micrograph of the Al-7Si-0.3Mg cast at the higher die temperature with an addition of 6wt.% EEM and showing a shear band near casting surface. Dark grey regions are eutectic, and the brighter regions are primary α-Al. b) Cross-section of the Al-7Si-0.3Mg cast at the higher die temperature with an addition of 7wt.% EEM containing a V-shape porosity band. Black regions are porosity at the casting centre. Dashed lines show the position of the die wall during filling.

3.3 Mechanical properties

The effects of magnesium and heat treatment in the tensile properties of SSM castings are shown in Figure 23. The offset yield strength increased with the increase of magnesium content of the alloy after T5 and T6 heat treatments. The offset yield strength obtained for the castings in the T6 condition is significantly higher compared to the T5 condition, for similar magnesium content. However, the offset yield strength also increases after T5 heat treatment compared to as-cast condition, as shown in Figure 23 for the Al-7Si-0.3Mg alloy. This indicates that precipitation hardening occurs during aging treatment, even for such a low magnesium concentration measured in the interior of the α_1-Al globules for the Al-7Si-0.3Mg casting in the T5 condition, as shown in Figure 13. The higher concentrations of magnesium and silicon measured at the edges of the α_1-Al globules, 0.04±0.01 and 1.90±0.20wt.% respectively, may contribute for the increase of offset yield strength during artificial aging to achieve T5 condition. The offset yield strength obtained for the castings in the T5 and T6 conditions show a good correlation to the magnesium concentration measured in the interior of the α_1-Al globules, as seen in Figure 23, and Figure 13, respectively.
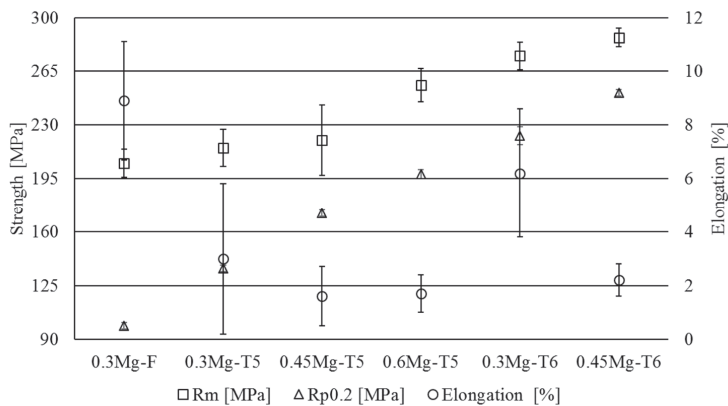
Figure 23: Influence of magnesium content and heat treatment in the $R_p0.2$, R_m and %elongation to fracture of the SSM castings.

The tensile strength was similar for the Al-7Si-0.3Mg casting in the as-cast and T5 conditions. For the castings in the T5 condition, the tensile strength just increased when the magnesium content increased to 0.6wt.%. In the T6 condition, the tensile strength increased with the increase of the magnesium content of the alloy.

The %elongation obtained for all castings in the T5 condition was similar. The %elongation obtained for the Al-7Si-0.3Mg casting in the T6 condition was higher compared to the T5 condition. This is most likely the result of the π-$Al_8FeMg_3Si_6$ phase transformation into very fine and small β-Al_5FeSi platelets, as shown in Figure 16. For the T6 condition, the %elongation decreased with the increase of magnesium content of the alloy. This decrease of ductility with the increase of magnesium may be the result of the larger volume fraction of π-$Al_8FeMg_3Si_6$ that remains in the microstructure of the Al-7Si-0.45Mg casting compared to the Al-7Si-0.3Mg casting

after solution treatment [55]. However, for the Al-7Si-0.45Mg casting, the %elongation was similar in both T5 and T6 conditions. The Al-7Si-0.3Mg castings showed larger scatter in the %elongation values in comparison to the Al-7Si-0.45Mg and Al-7Si-0.6Mg castings., as shown in Figure 23. This may indicates that more defects were obtained in the castings produced from the Al-7Si-0.3Mg alloy.

CONCLUSIONS

In this chapter the main conclusions are summarized.

Effect of grain refinement on slurry formation

In this thesis the effect of grain refinement on α_1-Al grain size, shape factor and solid fraction was studied. The results showed that the grain size and shape factor was similar for the refined and unrefined alloys. Additionally, the solid fraction obtained in the Rheometal™ slurry preparation process decreases slightly with the addition of grain refiners, from 0.31±0.04 for the unrefined alloy to 0.28±0.01 and 0.24±0.02 for the Al-8B and Al-5Ti-1B refined alloys, respectively.

It was observed in some of the α-Al globules evidence of liquid penetration suggesting that disintegration of α-Al globules by liquid wetting of the deformed crystals can occur during the Rheometal™ casting process.

Effect of magnesium on intermetallic phases formation and dissolution

π-$Al_8Mg_3FeSi_6$ phase was detected in the eutectic regions of all Al-7Si-Mg castings in as-cast and T5 conditions. For magnesium contents larger than 0.3wt.%, the Mg_2Si phase form in the eutectic regions in addition to the π-$Al_8Mg_3FeSi_6$ phase during solidification. The results suggest that high cooling rates favour the formation of the π-$Al_8Mg_3FeSi_6$ phase instead of the β-Al_5FeSi phase of Al-7Si-Mg SSM casting.

After T6 heat treatment most of the π-$Al_8Mg_3FeSi_6$ phase transformed into very fine β-Al_5FeSi phase and released magnesium into solid solution for the Al-7Si-0.3Mg SSM casting. However, for the Al-7Si-0.45Mg SSM casting π-$Al_8Mg_3FeSi_6$ phase remains in the microstructure and just a very few β-Al_5FeSi is detected.

Effect of grain refinement and casting parameters on segregation

A finer and more uniform microstructure was obtained near casting surface for the grain refined castings in comparison to the unrefined. The silicon content of the surface segregation layer was lower for the alloy refined with Al-5Ti-1B compared to the unrefined alloy, most likely due to the lower α_1-Al solid fraction obtained for the refined alloy.

Increasing the die temperature and decrease of EEM wt.% addition result in formation of shear bands close to the casting surface. In these conditions, porosity is observed in the interior of the V-shape bands formed in the casting centre. The V-shape bands were detected in all conditions. The decrease of die temperature and increase of EEM wt.% addition result in a V-shape band filled with eutectic.

Effect of magnesium on heat treatment response

The comparison of the magnesium concentration in the interior of the α_1-Al globules to the offset yield strength obtained for the SSM castings show that the offset yield strength increases with the increase of magnesium concentration in α_1-Al globules. Consequently, a larger offset yield strength was obtained for the castings in the T6

condition in comparison to the T5 condition. The low hardening response of the SSM castings in T5 condition compared to the T6 condition is suggested to result from the low magnesium solubility in α-Al at temperatures in the freezing range of the Al-7Si-Mg alloys.

The %elongation obtained for the Al-7Si-0.3Mg SSM castings in the T6 condition was higher in comparison to the T5 condition. However, for the Al-7Si-0.45Mg SSM the %elongation was similar in both heat treatment conditions.

CHAPTER 5
FUTURE WORK

CHAPTER INTRODUCTION

In this chapter, ideas that emerged from this work to improve the current knowledge are presented.

The results of this study suggest that α_1-Al grain size and shape factor are not influenced by grain refinement addition. The refinement of α_1-Al is advantageous to improve feeding, microstructure uniformity and fatigue resistance of the SSM castings. Therefore, the study of the influence of Rheometal™ process parameters and the addition of a solute element with high growth restriction can be beneficial.

A deeper understanding of the formation mechanisms of the surface segregation layer, shear bands and V-shape central bands is critical to produce SSM castings that can withstand high loads in service. The control of oxides during the Rheometal™ slurry preparation process is also critical for the casting mechanical and fatigue properties.

Fatigue is the cause of most component failures in service, therefore, the understanding of the influence of different parameters such as heat treatment, magnesium content, α_1-Al grain size on fatigue resistance of SSM castings is relevant. Additionally, the fracture analysis of fatigue tested samples can give information of the most critical defects that causes crack initiation in SSM castings.

REFERENCES

[1]   D.B. Spencer, R. Mehrabian, M.C. Flemings, Rheological behavior of Sn-15 pct Pb in the crystallization range, Metall. Trans. 3 (1972) 1925–1932. doi:10.1007/BF02642580.

[2]   M.C. Flemings, Behavior of metal alloys in the semisolid state, Metall. Trans. B. 22 (1991) 269–293. doi:10.1007/BF02651227.

[3]   X.G. Hu, Q. Zhu, H.V. Atkinson, H.X. Lu, F. Zhang, H.B. Dong, Y.L. Kang, A time-dependent power law viscosity model and its application in modelling semi-solid die casting of 319s alloy, Acta Mater. 124 (2017) 410–420. doi:10.1016/J.ACTAMAT.2016.11.031.

[4]   H. Atkinson, Semi-solid processing of metallic materials, Mater. Sci. Technol. 26:12 (2010) 1401–1413. doi:10.1179/026708310X12815992418012.

[5]   X.G. Hu, Q. Zhu, S.P. Midson, H.V. Atkinson, H.B. Dong, F. Zhang, Y.L. Kang, Blistering in semi-solid die casting of aluminium alloys and its avoidance, Acta Mater. 124 (2017) 446–455. doi:10.1016/J.ACTAMAT.2016.11.032.

[6]   S. Cecchel, D. Chindamo, M. Collotta, G. Cornacchia, A. Panvini, G. Tomasoni, M. Gadola, Lightweighting in light commercial vehicles : cradle-to-grave life cycle assessment of a safety-relevant component, Int. J. Life Cycle Assess. (2018). doi:10.1007/s11367-017-1433-5.

[7]   M. Blad, B. Johannesson, P. Nordberg, J. Winklhofer, M. Blad, B. Johannesson, P. Nordberg, Manufacturing and Fatigue Verification of Two Different Components Made by Semi-Solid Processing of Aluminium TX630 Alloy, in: Semi-Solid Process. Alloy. Compos. XIV, Trans Tech Publications, 2016: pp. 328–333. doi:10.4028/www.scientific.net/SSP.256.328.

[8]   Q.G. Wang, C.J. Davidson, Solidification and precipitation behaviour of Al-Si-Mg casting alloys, J. Mater. Sci. 36 (2001) 739–750.

[9]   O. Granath, M. Wessén, H. Cao, Determining effect of slurry process parameters on semisolid A356 alloy microstructures produced by RheoMetal process, Int. J. Cast Met. Res. 21 (2008) 349–356. doi:10.1179/136404608X320706.

[10]   M. Yildirim, D. Özyürek, The effects of Mg amount on the microstructure and mechanical properties of Al-Si-Mg alloys, Mater. Des. 51 (2013) 767–774. doi:10.1016/j.matdes.2013.04.089.

[11]   R. Chen, Q. Xu, H. Guo, Z. Xia, Q. Wu, B. Liu, Correlation of solidification microstructure refining scale, Mg composition and heat treatment conditions with mechanical properties in Al-7Si-Mg cast aluminum alloys, Mater. Sci. Eng. A. 685 (2017) 391–402. doi:10.1016/j.msea.2016.12.051.

[12]   E. Sjölander, S. Seifeddine, Optimization of solution treatment of cast Al-7Si-0.3Mg and Al-8Si-3Cu-0.5Mg alloys, Metall. Mater. Trans. A Phys. Metall. Mater. Sci. 45 (2014) 1916–1927. doi:10.1007/s11661-013-2141-9.

[13] S. Menargues, E. Martín, M.T. Baile, J.A. Picas, New short T6 heat treatments for aluminium silicon alloys obtained by semisolid forming, Mater. Sci. Eng. A. 621 (2015) 236–242. doi:10.1016/j.msea.2014.10.078.

[14] J.A. Taylor, J. Barresi, M.J. Couper, D.H. StJohn, Influence of Mg Content on the Microstructure and Solid Solution Chemistry of Al-7%Si-Mg Casting Alloys During Solution Treatment, in: Alum. Alloy. - Their Phys. Mech. Prop., Trans Tech Publications, 2000: pp. 277–282.

[15] J.A. Taylor, Iron-containing intermetallic phases in Al-Si based casting alloys, Procedia Mater. Sci. 1 (2012) 19–33. doi:10.1016/j.mspro.2012.06.004.

[16] E.A. Elsharkawi, E. Samuel, A.M. Samuel, F.H. Samuel, Effects of Mg, Fe, Be additions and solution heat treatment on the π-AlMgFeSi iron intermetallic phase in Al-7Si-Mg alloys, J. Mater. Sci. 45 (2010) 1528–1539. doi:10.1007/s10853-009-4118-z.

[17] N.A. Belov, D.G. Eskin, A.A. Aksenov, Multicomponent Phase Diagrams: Applications for Commercial Aluminum Alloys, Elsevier B.V., 2005.

[18] Thermo-Calc Software 2016b with TCAL2 database Al-alloys, Thermo-Calc Software AB, Stockholm, Sweden, (n.d.).

[19] R.I. Mackay, J.E. Gruzleski, Quantification of iron in aluminium-silicon foundry alloys via thermal analysis, Int. J. Cast Met. Res. 10 (1997) 131–145. doi:10.1080/13640461.1997.11819228.

[20] K.Y. Wen, W. Hu, G. Gottstein, Intermetallic compounds in thixoformed aluminium alloy A356, Mater. Sci. Technol. 19 (2003) 762–768. doi:10.1179/026708303225002839.

[21] L. Bäckerud, G. Chai, J. Tamminen, Solidification Characteristics of Aluminum Alloys, Volume 2: Foundry Alloys, in: AFS/SCANALUMINIUM, AFS/SKANALUMINIUM, Stockholm, 1990: pp. 135–141.

[22] F.H. Samuel, A.M. Samuel, P. Ouellet, H.W. Doty, Effect of Mg and Sr additions on the formation of intermetallics in Al-6 wt pct Si-3.5 wt pct Cu-(0.45) to (0.8) wt pct Fe 319-type alloys, Metall. Mater. Trans. A. 29 (1998) 2871–2884. doi:10.1007/s11661-998-0194-y.

[23] L. Lu, A.K. Dahle, Iron-rich intermetallic phases and their role in casting defect formation in hypoeutectic Al-Si alloys, Metall. Mater. Trans. A Phys. Metall. Mater. Sci. 36 (2005) 819–835. doi:10.1007/s11661-005-1012-4.

[24] L. Liu, A.M.A. Mohamed, A.M. Samuel, F.H. Samuel, H.W. Doty, S. Valtierra, Precipitation of β-Al5FeSi Phase Platelets in Al-Si Based Casting Alloys, Metall. Mater. Trans. A. 40 (2009) 2457–2469. doi:10.1007/s11661-009-9944-8.

[25] L.A. Narayanan, F.H. Samuel, J.E. Gruzleski, Crystallization behavior of iron-containing intermetallic compounds in 319 aluminium alloy, Met. Mat. Trans. A. 25 (1994) 1761–1773. doi:10.1007/BF02668540.

[26] D.G. McCartney, Grain refining of aluminium and its alloys using inoculants, Int. Mater. Rev. 34 (1989) 247–260.

[27] M.A. Easton, M. Qian, A. Prasad, D.H. StJohn, Recent advances in grain refinement of light metals and alloys, Curr. Opin. Solid State Mater. Sci. 20 (2015) 13–24. doi:10.1016/j.cossms.2015.10.001.

[28] T.E. Quested, Understanding mechanisms of grain refinement of aluminium alloys by inoculation, Mater. Sci. Technol. 20 (2004) 1357–1369. doi:10.1179/026708304225022359.

[29] Y. Birol, Effect of silicon content in grain refining hypoeutectic Al–Si foundry alloys with boron and titanium additions, Mater. Sci. Technol. 28 (2012) 385–389. doi:10.1179/1743284711Y.0000000049.

[30] Z. Chen, H. Kang, G. Fan, J. Li, Y. Lu, J. Jie, Y. Zhang, T. Li, X. Jian, T. Wang, Grain refinement of hypoeutectic Al-Si alloys with B, Acta Mater. 120 (2016) 168–178. doi:10.1016/j.actamat.2016.08.045.

[31] D. Qiu, J.A. Taylor, M.X. Zhang, P.M. Kelly, A mechanism for the poisoning effect of silicon on the grain refinement of Al-Si alloys, Acta Mater. 55 (2007) 1447–1456. doi:10.1016/j.actamat.2006.09.046.

[32] A.M. Samuel, F.H. Samuel, S. Valtierra, A metallographic study of grain refining of Sr-modified 356 alloy, Int. J. Met. (2016). doi:10.1007/s40962-016-0075-x.

[33] L. Lu, A.K. Dahle, Effects of combined additions of Sr and AlTiB grain refiners in hypoeutectic Al-Si foundry alloys, Mater. Sci. Eng. A. 435–436 (2006) 288–296. doi:10.1016/j.msea.2006.07.081.

[34] J.A. Yurko, R.A. Martinez, M.C. Flemings, Commercial development of the Semi-Solid Rheocasting (SSR) process, Metall. Sci. Technol. 21 (2003) 39.

[35] T. Chucheep, J. Wannasin, R. Canyook, T. Rattanochaikul, S. Janudom, S. Wisutmethangoon, M.C. Flemings, Characterization of flow behavior of semi-solid slurries with low solid fractions, Metall. Mater. Trans. A Phys. Metall. Mater. Sci. 44 (2013) 4754–4763. doi:10.1007/s11661-013-1819-3.

[36] M. Wessén, H. Cao, The RSF technology; A possible breakthrough for semi-solid casting processes, Int. Conf. High Tech Die Cast. (2006).

[37] D. Doutre, G. Hay, P. Wales, J.-P. Gabathuler, Seed: a New Process for Semi-Solid Forming, Can. Metall. Q. 43 (2004) 265–272. doi:10.1179/cmq.2004.43.2.265.

[38] Z. Yang, J.W. Bae, C.G. Kang, Effect of Vertical Electromagnetic Stirring on the Grain Refinement of A356 Aluminum Alloy Inoculated by Al-5Ti-B, Solid State Phenom. 116–117 (2006) 344–349. doi:10.4028/www.scientific.net/SSP.116-117.344.

[39] M.A. Easton, H. Kaufmann, W. Fragner, The effect of chemical grain refinement and low superheat pouring on the structure of NRC castings of aluminium alloy Al-7Si-0.4Mg, Mater. Sci. Eng. A. 420 (2006) 135–143.

[40] Z. Fan, Semisolid metal processing, Int. Mater. Rev. 47 (2002) 49–85. doi:10.1179/095066001225001076.

[41] T. Haga, P. Kapranos, Simple rheocasting processes, J. Mater. Process. Technol. 130–131 (2002) 594–598. doi:10.1016/S0924-0136(02)00819-1.

[42] M. Payandeh, M.H. Sabzevar, A.E.W. Jarfors, M. Wessén, Solidification and Re-melting Phenomena during the Slurry Preparation Stage using the RheoMetal TM Process, Metall. Mater. Trans. B. (2017) 1–22. doi:10.1007/s11663-017-1061-2.

[43] M. Payandeh, A.E.W. Jarfors, M. Wessén, Solidification Sequence and Evolution of Microstructure During Rheocasting of Four Al-Si-Mg-Fe Alloys with Low Si Content, Metall. Mater. Trans. A Phys. Metall. Mater. Sci. 47 (2016) 1215–1228. doi:10.1007/s11661-015-3290-9.

[44] M. Payandeh, A.E.W. Jarfors, M. Wessén, Effect of superheat on melting rate of EEM of Al alloys during stirring using the RheoMetal process, Solid State Phenom. (2013) 392–397.

[45] M. Hitchcock, Y. Wang, Z. Fan, Secondary solidification behaviour of the Al-Si-Mg alloy prepared by the rheo-diecasting process, Acta Mater. 55 (2007) 1589–1598. doi:10.1016/j.actamat.2006.10.018.

[46] G. Govender, H. Möller, Evaluation of Surface Chemical Segregation of Semi-Solid Cast Aluminium Alloy A356, Solid State Phenom. 143 (2008) 433–438.

[47] S. Otarawanna, C.M. Gourlay, H.I. Laukli, A.K. Dahle, Formation of the surface layer in hypoeutectic Al-alloy high-pressure die castings, Mater. Chem. Phys. 130 (2011) 251–258. doi:10.1016/j.matchemphys.2011.06.035.

[48] C.M. Gourlay, A.K. Dahle, Dilatant shear bands in solidifying metals, Nature. 445 (2007) 70–73. doi:10.1038/nature05426.

[49] S. Otarawanna, C.M. Gourlay, H.I. Laukli, A.K. Dahle, Microstructure formation in AlSi4MgMn and AlMg5Si2Mn high-pressure die castings, Metall. Mater. Trans. A Phys. Metall. Mater. Sci. 40 (2009) 1645–1659. doi:10.1007/s11661-009-9841-1.

[50] M. Payandeh, A.E.W. Jarfors, M. Wessén, Influence of microstructural inhomogeneity on fracture behaviour in SSM-HPDC Al-Si-Cu-Fe component with low Si content, Solid State Phenom. 217–218 (2014) 67–74. doi:10.4028/www.scientific.net/SSP.217-218.67.

[51] C.M. Gourlay, H.I. Laukli, A.K. Dahle, Defect band characteristics in Mg-Al and Al-Si high-pressure die castings, Metall. Mater. Trans. A. 38 (2007) 1833–1844. doi:10.1007/s11661-007-9243-1.

[52] H. Möller, E.P. Masuku, The Influence of Liquid Surface Segregation on the Pitting Corrosion Behavior of Semi-Solid Metal High Pressure Die Cast Alloy F357, Open Corros. J. 2 (2009) 216–220.

[53] H. Möller, G. Govender, W.E. Stumpf, P.C. Pistorius, Comparison of heat treatment response of semisolid metal processed alloys A356 and F357, Int. J. Cast Met. Res. 23 (2010) 37–43. doi:10.1179/174313309X451252.

[54] J.Y. Yao, J.A. Taylor, Characterisation of intermetallic particles formed during solution treatment of an Al–7Si–0.4Mg–0.12Fe alloy, J. Alloys Compd. 519 (2012) 60–66. doi:10.1016/j.jallcom.2011.12.047.

[55] C.H. Caceres, C.J. Davidson, Q.G. Wang, J.R. Griffiths, The effect of Mg on the microstructure and mechanical behavior of Al-Si-Mg casting alloys, Metall. Mater. Trans. A. 30 (1999) 2611–2618. doi:10.1007/s11661-999-0301-8.

[56]   H. Möller, G. Govender, W. Stumpf, The T5 Heat Treatment of Semi-Solid Metal Processed Aluminium Alloy F357, Mater. Sci. Forum. 618–619 (2009) 365–368. doi:10.4028/www.scientific.net/MSF.618-619.365.

[57]   M. Rosso, I. Peter, R. Villa, Effects of T5 and T6 Heat Treatments Applied to Rheocast A356 Parts for Automotive Applications, Solid State Phenom. 141–143 (2008) 237–242. doi:10.4028/www.scientific.net/SSP.141-143.237.

[58]   J. Wannasin, R. Canyook, S. Wisutmethangoon, M.C. Flemings, Grain refinement behavior of an aluminum alloy by inoculation and dynamic nucleation, Acta Mater. 61 (2013) 3897–3903. doi:10.1016/j.actamat.2013.03.029.

[59]   K.T. Kashyap, T. Chandrashekar, Effects and mechanisms of grain refinement in aluminium alloys, Bull. Mater. Sci. 24 (2001) 345–353. doi:10.1007/BF02708630.

[60]   ASTM, Standard Test Method for Determining Volume Fraction by Systematic Manual Point Count, Practice. (2011) 1–7. doi:10.1520/E0562-11.2.

[61]   L. Gao, Y. Harada, S. Kumai, Microstructural characterization of aluminum alloys using Weck's reagent, part II: Coloring mechanism, Mater. Charact. 107 (2015) 434–452. doi:10.1016/j.matchar.2015.05.006.

[62]   L. Gao, Y. Harada, S. Kumai, Analysis of microstructure evolution and precise solid fraction evaluation of A356 aluminum alloy during partial re-melting by a color etching method, J. Mater. Sci. 47 (2012). doi:10.1007/s10853-012-6586-9.

[63]   H.I. Laukli, C.M. Gourlay, A.K. Dahle, Migration of crystals during the filling of semi-solid castings, Metall. Mater. Trans. A Phys. Metall. Mater. Sci. 36 (2005) 805–818. doi:10.1007/s11661-005-1011-5.

[64]   SS-EN-ISO 6892-1:2016 Metallic materials - Tensile testing - Part 1: Method of test at room temperature, 2016.

[65]   M. Yan, W. Luo, Effects of grain refinement on the rheological behaviors of semisolid hypoeutectic Al–Si alloys, Mater. Chem. Phys. 104 (2007) 267–270. doi:10.1016/j.matchemphys.2007.02.093.

[66]   A.. Sharma, R.. Gupta, L.. Ratke, Study of microstructure characteristics of Al-7%Si alloy cast through rheo-metal process, in: Mater. Sci. Technol. Conf. Exhib. 2014, MS T 2014, 2014: pp. 1243–1251.

[67]   B. Chalmers, The structure of ingots, J. Aust. Inst. Met. 8 (1963) 255–263.

[68]   S. Ji, Z. Fan, Solidification behavior of Sn-15 wt pct Pb alloy under a high shear rate and high intensity of turbulence during semisolid processing, Metall. Mater. Trans. A. 33 (2002) 3511–3520. doi:10.1007/s11661-002-0338-4.

[69]   H. Biloni, B. Chalmers, Origin of the equiaxed zone in small ingots, J. Mater. Sci. 3 (1968) 139–149. doi:10.1007/BF00585481.

[70]   S. Otarawanna, C.M. Gourlay, H.I. Laukli, A.K. Dahle, Agglomeration and bending of equiaxed crystals during solidification of hypoeutectic Al and Mg alloys, Acta Mater. 58 (2010) 261–271. doi:10.1016/j.actamat.2009.09.002.

[71] R.D. Doherty, H.-I. Lee, E.A. Feest, Microstructure of stir-cast metals, Mater. Sci. Eng. 65 (1984) 181–189. doi:10.1016/0025-5416(84)90211-8.

[72] S. Karagadde, P.D. Lee, B. Cai, J.L. Fife, M.A. Azeem, K.M. Kareh, C. Puncreobutr, D. Tsivoulas, T. Connolley, R.C. Atwood, Transgranular liquation cracking of grains in the semi-solid state, Nat. Commun. 6 (2015) 8300. doi:10.1038/ncomms9300.

[73] L. Pedersen, L. Arnberg, Anomalous microsegregation in Al–Si foundry alloys, Mater. Sci. Eng. A. 241 (1998) 285–289. doi:10.1016/S0921-5093(97)00490-5.

[74] A.K. Dahle, L. Arnberg, D. Appelian, Burst feeding and its role in porosity formation during solidification of Al foundry alloys, AFS Trans. 160 (1997) 963–970.

APPENDED PAPERS

Supplement I   Jorge Santos, Lothar H. Kallien, Anders E. W. Jarfors, Arne K. Dahle; Influence of grain refinement on slurry formation and surface segregation in Al-7Si-0.3Mg semi-solid castings.

Manuscript submitted for journal publication.

Supplement II   Jorge Santos, Anders E. W. Jarfors, Arne K. Dahle; The effect of magnesium on the intermetallic phases and heat treatment response of cast Al-7Si-Mg.

Manuscript.

Supplement III   Jorge Santos, Anders E. W. Jarfors, Arne K. Dahle; Filling, feeding and defect formation of thick-walled AlSi7Mg0.3 semi-solid castings.

Presented in the 14th International Conference on Semi Solid Processing of Alloys and Composites, October 23rd-27th, Salt Lake City, Utah, USA. Published in Solid State Phenomena, Trans Tech Publications, 2016. Vol. 256, pp. 222-227.